

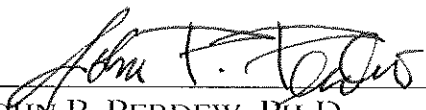
APPLYING AND ASSESSING SOME SEMI-LOCAL DENSITY FUNCTIONALS  
FOR CONDENSED MATTER PHYSICS AND QUANTUM CHEMISTRY

A DISSERTATION  
SUBMITTED ON THE THIRTIETH OF JANUARY, 2013  
TO THE DEPARTMENT OF PHYSICS AND ASTRONOMY  
OF THE SCHOOL OF SCIENCE AND ENGINEERING  
OF TULANE UNIVERSITY  
IN PARTIAL FULFILLMENT OF THE REQUIREMENTS  
FOR THE DEGREE OF  
DOCTOR OF PHILOSOPHY  
BY

---

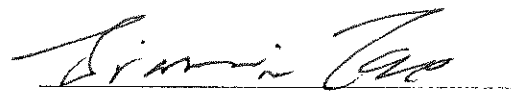
PAN HAO

APPROVED:

  
JOHN P. PERDEW, PH.D.  
CHAIRMAN

  
JAMES H. MCGUIRE, PH.D.

  
LEV KAPLAN, PH.D.

  
JIANMIN TAO, PH.D.



# Acknowledgements

I would like to thank my advisor Dr. Perdew for his guiding during the five years. He is a great person and scientist. He taught me the fundamental knowledge of density functional theory, supported me to do research, and helped me to be a qualified Ph.D student. I would also thank my committee members, Professor Dr. Tao, Dr. Kaplan, and Dr. McGuire for their comments and suggestions. I appreciate the contribution from Dr. Csonka, Dr. Philipson, Dr. Sun, Dr. Ruzsinszky, and my colleagues Bing and Yuan. I would thank my wife Ming and my parents for their supports and encouragements so that I can finish my degree.

# Contents

Acknowledgements.....	ii
List of Tables .....	v
List of Figures.....	vii
CHAPTER 1 INTRODUCTION .....	1
CHAPTER 2 DENSITY FUNCTIONAL THEORY.....	7
2.1 Wavefunction Theory .....	7
2.1.1 Wavefunction of Many-electron System .....	7
2.1.2 Schrödinger Equation and Wavefunction Variational Principle .....	9
2.1.3 Non-interacting System and Slater Determinant.....	10
2.1.4 Hellmann-Feynman Theorem .....	12
2.2 Definition of DFT .....	13
2.2.1 Hohenberg-Kohn Theorem and Constrained Search .....	13
2.2.2 Kohn-Sham Non-interacting System .....	15
2.2.3 Exchange Energy and Correlation Energy .....	18
2.2.4 Coupling-constant Integration and Exchange-correlation Hole.....	20
2.3 Semi-local Functionals.....	24
2.3.1 Uniform Electron Gas and LSDA .....	24
2.3.2 Slowly Varying Density and (meta-) GGA Approximation .....	29
2.3.3 Beyond the Semi-local Functional .....	32
2.4 Density Functional Perturbation Theory.....	33
2.4.1 Density Functional Perturbation Theory .....	33
2.4.2 Lattice Dynamics from Electronic-Structure Theory.....	37
2.4.3 Vibrational States in Crystalline Solids .....	38
2.5 Applying and Testing on Condensed Matter Physics and Quantum Chemistry .....	40
CHAPTER 3 LATTICE CONSTANTS FROM SEMI-LOCAL DENSITY FUNCTIONALS WITH ZERO-POINT PHONON CORRECTION .....	42
3.1 Introduction of Lattice Constant Calculation by Using First-Principle DFT with Zero- Point Energy Correction .....	42
3.2 The ZPAE Correction: From a Simple Model to a Phonon Model.....	45
3.3 Results and Discussions.....	49
3.3.1 Comparison of the Two ZPAE Corrections .....	49

3.3.2	Performance of Semi-Local Functionals for Lattice Constants .....	55
3.3.3	Self-Consistency Effect on the Lattice Constant Calculation .....	62
3.4	Conclusions.....	63
CHAPTER 4 PERFORMANCE OF META-GGA FUNCTIONALS ON GENERAL MAIN GROUP THERMOCHEMISTRY, KINETICS, AND NONCOVALENT INTERACTIONS .....		66
4.1	Introduction.....	66
4.2	Computation Details .....	70
4.3	Results and Discussion .....	71
4.3.1	The Mean Absolute Errors.....	71
4.3.2	Weighted Total Mean Absolute Error.....	84
4.3.3	Results with the Dispersion Correction .....	86
4.4	Conclusion and Summary .....	89
References.....		92

# List of Tables

1. The zero-point energy per atom (columns 1 and 2), the Grüneisen parameter (columns 3 and 4), and the lattice constant correction as a percentage of the experimental lattice constant using the simple model and phonon correction (columns 5 and 6, respectively). ..... 50
2. Test of revTPSS self-consistency employing the bond lengths (in angstroms) of the Li, N, and Ca dimers. .... 56
3. Theoretical lattice constants (in angstroms) calculated from BAND code using LSDA, PBE, PBEsol, TPSS, and revTPSS functionals. The revTPSS density is used for all calculations. The experimental lattice constants are corrected for ZPAE..... 57
4. Relative errors (in percent) in lattice constants with respect to the ZPAE-corrected experimental values, ordered from the most positive value to the least positive value of revTPSS. .... 59
5. Error statistics for the revTPSS lattice constant, compared with corrected experimental lattice constant using two different corrections, for the solids listed in Table 3, excepting Rb, HfC, HfN, VN and NbN for the phonon model. .... 61
6. The inter-layer equilibrium lattice constant (in angstroms) of graphite, calculated from BAND and VASP. .... 62
7. Lattice constants calculated (in angstroms) from the BAND and VASP code in revTPSS, self-consistently and from the LDA density. The difference between

them is presented as a possible measure of the self-consistency effect, which is expected to be largest in soft solids like these with BAND, but not VASP. ....	63
8. The mean absolute errors ( $\text{kcal mol}^{-1}$ ) of the basis sets compared to the basis-set limit for three smaller test sets using the revTPSS functional .....	71
9. The MAE or WTMAE of the discussed functionals for the MB08-165 subset, the miscellaneous properties group, the reaction energies, the noncovalent bonds and the total test set. ....	85
10. The WTMAE of the discussed functionals for different test sets with D3 correction in $\text{kcal mol}^{-1}$ . The D3 corrections for revTPSS, regTPSS, and MGGA_MS are those designed for TPSS, and are not optimal for other functionals, especially MGGA_MS. ....	87

# List of Figures

1. The self-consistent loop for solving K-S equation ..... 18
2. The self-consistent loop for solving the linear perturbation equation ..... 36
3. (Color online) The light gray (green) line is the ratio of the zero-point energy approximated by the Debye model to that computed from the phonon average frequency. The dark gray (red) line is the ratio of the lattice constant correction ( $\Delta a$ ) alculated by the simple model to that calculated by the phonon model. .... 52
4. (Color online) The light gray (blue) line is the ratio of the Gruneisen parameter approximated by the Dugdale-MacDonald model to that approximated by the phonon model. The dark gray (red) line is the ratio of the lattice constant correction ( $\Delta a$ ) calculated by the simple model to that calculated by the phonon model. Note the similarity of the two curves, which shows that most of the error of the simple model arises from the Dugdale-MacDonald approximation..... 54
5. MAEs of PBE, TPSS, revTPSS, regTPSS, MGGA\_MS, M06L and B3LYP for the eight subsets of the miscellaneous properties group in GMTKN30 database. A number under the name of a subset in a bracket indicates the number of entries of the subset..... 75



6. MAEs of PBE, TPSS, revTPSS, regTPSS, MGGA\_MS, M06L and B3LYP for the reaction group in GMTKN30 database. A number under the name of a subset in a bracket indicates the number of entries of the subset. .... 79
7. MAEs of PBE, TPSS, revTPSS, regTPSS, MGGA\_MS, M06L and B3LYP for the noncovalent interaction group in GMTKN30 database. A number under the name of a subset in a bracket indicates the number of entries of the subset..... 83

# CHAPTER 1

## INTRODUCTION

It has been more than one century since people discovered that the electron is one of the elementary particles constructing our world. Electrons have negative charges which work as glue to hold the atoms together in molecules and solids. The interactions between electrons and nuclei are mainly Coulomb interactions. The mass of an electron is very small, approximately  $1/1846$  of a proton. The momentum of an electron is also small, so it cannot be found fully localized because of the uncertainty principle. The wave-like quantum property of electrons balances the attraction from nuclei and prevents them from collapsing into nuclei. Quantum mechanics was formulated to describe the microscopic picture of a physical system. Including the fermion character of electrons that leads to Pauli exclusion principle, all the fundamental laws necessary for mathematical treatment of an electronic system were known in 1930s. The only challenge left to people is how to solve the complex equations derived from these laws.

In quantum mechanics, an electronic system can be described by using the Schrödinger equation. The time-independent Hamiltonian of the system can be expressed as

$$\begin{aligned}\hat{H} = & -\frac{\hbar^2}{2m_e} \sum_{i=1}^N \nabla_i^2 + \sum_{i,I} \frac{-Z_I e^2}{|\mathbf{r}_i - \mathbf{R}_I|} + \frac{1}{2} \sum_{j \neq i} \frac{e^2}{|\mathbf{r}_i - \mathbf{r}_j|} \\ & -\frac{\hbar^2}{2M_I} \sum_I \nabla_I^2 + \frac{1}{2} \sum_{I \neq J} \frac{Z_I Z_J e^2}{|\mathbf{R}_I - \mathbf{R}_J|},\end{aligned}\tag{1-1}$$

where electrons with mass  $m_e$  are denoted by lower case letters and nuclei, with positive charge  $Z_I$  and mass  $M_I$ , are denoted by upper case letters.  $\hbar$  is Plank's constant and  $e$  is the elementary charge. By solving the Schrödinger equation

$$\hat{H}\Psi = E\Psi,\tag{1-2}$$

we can get the eigenstates of the system and then predict its behavior. Among all the solved states, the lowest-energy state is the ground state and other states are excited states. The ground state is important for quantum chemistry and condensed matter physics because it is related to many properties, such as cohesive energy, reaction energy, reaction barriers heights, charge density, equilibrium crystal structure, nuclear vibrations, electronic band structure, magnetic susceptibilities and phase transitions. The knowledge of the ground state is essential for studying excited states. Here we will only consider ground state.

The exact eigenstate of the Schrödinger equation (1-2) is difficult to solve since the electrons and nuclei are coupled together. Because the nuclei are much heavier than electrons, the motion of the nuclei is on a time scale much larger than typical electronic scales. The Born-Oppenheimer or adiabatic approximation [1] assumes that the electrons are in their instantaneous ground state as the nuclei move. Without considering the motion of nuclei, the eigenstate of the Schrödinger equation only has the wavefunction of

electrons. The approximation rationally separates the coupled electron-nucleus system and makes the calculation easier. In this case, when we consider the motion of nuclei, we can treat nuclei as classic particles. With solved electron wavefunction, the electrostatic force acting on nuclei can be calculated.

Within the Born-Oppenheimer approximation and adopting Hartree atomic units  $\hbar = m_e = e = 4\pi\epsilon_0=1$ , the Hamiltonian of electrons can be written as

$$\begin{aligned}\hat{H} &= -\frac{1}{2}\sum_{i=1}^N \nabla_i^2 + \sum_{i=1}^N v(\mathbf{r}_i) + \frac{1}{2}\sum_i \sum_{j \neq i} \frac{1}{|\mathbf{r}_i - \mathbf{r}_j|} \\ &= \hat{T} + \hat{V}_{ext} + \hat{V}_{ee} \quad ,\end{aligned}\tag{1-3}$$

which is simpler compared to the previous equation. It is still difficult to solve the many-electron system even though we have advanced computer technology. There are some commonly used wavefunction approaches to accurately compute correlation efforts, such as configuration-interaction [2], many-body perturbation theory [3-5], and Quantum Monte Carlo methods[6, 7]. The wavefunction  $\Psi(\mathbf{r}_1\sigma_1, \dots, \mathbf{r}_N\sigma_N)$  describing a system of  $N$  electrons has arguments of electron positions and spins. The number of the arguments is linear with the number of electrons  $N$ . As  $N$  increases, the effort required to find the wavefunction exponentially scales up. The wavefunction of electrons is antisymmetric, which can largely reduce the effort to solve wavefunction. However, wavefunction approaches are still computationally expensive and are only limited to relatively small systems.

A wavefunction contains all the information of a quantum system, but it is not observable. Moreover, the computational cost is expensive. Hartree-Fock method uses a Slater determinant, a determinant of one-particle orbitals, instead of wavefunction. In this

method, the kinetic energy and exchange energy could be exactly expressed for given non-interacting electron orbitals. But there is no correlation energy considered in Hartree-Fock method. So for some properties that could be affected by the correlation, such as atomization energy, the performance of the Hartree-Fock is bad [8].

Another approach is to use electron density functional instead of wavefunction functional. Electron density is a measurable quantity in a three dimensional space. The study of density functional dated back in 1920s. Thomas and Fermi first used the electron density to calculate the energy of a system. Even though they did not give the right kinetic energy functional and missed exchange energy, it was an important step. Later, Dirac added an exchange part to the previous model and built the Thomas-Fermi-Dirac model. In the later version, some correlation energy was added. In 1960s, there were some significant progresses in density functional theory (DFT). In 1964, Hohenberg and Kohn [9] proved that DFT is an exact approach to study many-electron systems. In 1965, Kohn and Sham (KS) [10] proposed a scheme that separates the exchange-correlation energy from the large kinetic energy and Hartree energy. In KS scheme (we will use DFT to refer to the KS scheme), the only part that needs to be approximated is the relatively small exchange-correlation energy. DFT has the same computational scheme as the Hartree-Fock method that each electron is subjected to an effective potential created by all other particles. The success of DFT benefits from uniform electron gas, which could be a real physical system and has analytical expression for the exchange-correlation energy. Inclusion of correlation energy makes DFT perform better than the Hartree-Fock method.

After many-year development, there is a huge variety of exchange-correlation functionals. From the easiest density functional local density approximations (LDA), which was originally designed for solid state physics, to other higher-level functionals that work better for quantum chemistry, the functionals are getting more sophisticated and also more general. They can work for different systems because they satisfy more constraints. In the meantime, they can be reduced to LDA in the uniform electron gas limit. On the other hand, some useful theories, like density functional perturbation theory (DFPT) [11], have been developed based on DFT. Many physical properties depend upon a system response to some form of perturbation. e.g., polarizabilities, phonons, Raman and infra-red spectra, etc. DFPT is a powerful and flexible theoretical technique that allows calculation of such properties within the density functional framework. In Chapter 2, we will review wavefunction theory, density functional theory, and density functional perturbation theory.

In Chapter 3, we will apply DFT and DFPT to calculate the lattice constants of 58 cubic solids and graphite. The crystal structure is emphasized by the solid state physicists and material scientists. In a standard Kohn-Sham density functional calculation, the total energy of a crystal at zero temperature can be evaluated for a perfect static lattice of nuclei and minimized with respect to the lattice constant. Semi-local functionals are widely used for solids, because they are often nonempirical and are computationally faster than non-local functionals. Therefore the functional of LDA and generalized gradient approximation (GGA) are often used to study periodic solids. We will present the performances of some semi-local functionals - LDA, PBE, PBEsol, TPSS, and revTPSS. A zero-point vibrational energy of a crystal, whose anharmonicity expands

equilibrium lattice constant, is ignored in DFT calculation because of Born-Oppenheimer approximation. The zero-point energy can be used to correct the calculated lattice constant or correct the experimental reference value for the lattice constant to that for a static lattice. We will use DFPT to calculate the zero-point energy and then compare it to a simple model that is based on the Debye and Dugdale-MacDonald approximations. The lattice constant calculated from DFT will be compared with an experimental value that is corrected to that of static lattice.

In Chapter 4, we will assess performance of some meta-generalized-gradient approximation (meta-GGA) functionals on a big molecular set. Among the computationally efficient semi-local density functionals for the exchange-correlation energy, meta-GGAs are potentially the most accurate. In recent years, Perdew's group has developed some new meta-GGAs, revised Tao-Perdew-Staroverov-Scuseria (revTPSS), regularized revTPSS or regTPSS, and meta-GGA made simple or MGGA\_MS. We assessed these functionals within and beyond their "comfort zones", on Grimme's big test set, called GMTKN30, of main-group molecular energetics (thermochemistry, kinetics, and noncovalent interactions). GMTKN30 is a large main-group molecular energy test set composed of 30 smaller test sets and covers a large cross section of chemically relevant properties, and thus can give a comprehensive main-group molecular evaluation and assessment for a tested functional. We also compared these new functionals against the standard Perdew-Burke-Ernzerhof (PBE) GGA, TPSS and Minnesota M06L meta-GGAs, and Becke-3-Lee-Yang-Parr (B3LYP) hybrid of GGA with exact exchange.

# CHAPTER 2

## DENSITY FUNCTIONAL THEORY

### 2.1 Wavefunction Theory

#### 2.1.1 Wavefunction of Many-electron System

In an electronic system, an electronic state can be expressed as a wavefunction  $\Psi(\mathbf{r}_1\sigma_1, \dots, \mathbf{r}_N\sigma_N)$ .  $|\Psi(\mathbf{r}_1\sigma_1, \dots, \mathbf{r}_N\sigma_N)|^2$  corresponds to probability density of finding electron 1 at position  $\mathbf{r}_1$  with spin  $\sigma_1, \dots$ , and electron  $N$  at position  $\mathbf{r}_N$  with spin  $\sigma_N$ . The wavefunction satisfies normalization condition

$$\sum_{\sigma_1, \dots, \sigma_N} \int d^3r_1 \dots d^3r_N |\Psi(\mathbf{r}_1\sigma_1, \dots, \mathbf{r}_N\sigma_N)|^2 = \langle \Psi | \Psi \rangle = 1. \quad (2-1)$$

Because electrons are indistinguishable fermions, the wavefunction is antisymmetric when we exchange any two electrons

$$\Psi(\mathbf{r}_1\sigma_1, \dots, \mathbf{r}_i\sigma_i, \dots, \mathbf{r}_j\sigma_j, \dots, \mathbf{r}_N\sigma_N) = -\Psi(\mathbf{r}_1\sigma_1, \dots, \mathbf{r}_j\sigma_j, \dots, \mathbf{r}_i\sigma_i, \dots, \mathbf{r}_N\sigma_N). \quad (2-2)$$

There are  $N!$  distinct permutations of the labels  $1, 2, \dots, N$ , which by (2-2) all have same  $|\Psi|^2$ . Thus  $N! |\Psi(\mathbf{r}_1\sigma_1, \dots, \mathbf{r}_N\sigma_N)|^2$  is the probability density of finding any electron at position  $\mathbf{r}_1$  with spin  $\sigma_1, \dots$ , and any electron at position  $\mathbf{r}_N$  with  $\sigma_N$ .



A wavefunction has all information of an electronic state in an electronic system. It can be used to calculate not only the density, but also the energies and potentials of electrons. The  $n$ -th order electron matrix can be defined as [12]

$$\rho_n(\mathbf{r}_1\sigma_1 \dots \mathbf{r}_n\sigma_n, \mathbf{r}_1\sigma_1 \dots \mathbf{r}_n\sigma_n) \equiv \binom{N}{n} \sum_{\sigma_{n+1}, \dots, \sigma_N} \int d^3r_{n+1} \dots d^3r_N \Psi^*(\mathbf{r}_1\sigma_1 \dots \mathbf{r}_n\sigma_n \mathbf{r}_{n+1}\sigma_{n+1}, \dots, \mathbf{r}_N\sigma_N) \Psi(\mathbf{r}_1\sigma_1 \dots \mathbf{r}_N\sigma_N), \quad (2-3)$$

where  $\binom{N}{n}$  is a binomial coefficient. In particular, the first order electron matrix is

$$\rho_1(\mathbf{r}\sigma, \mathbf{r}\sigma) = N \sum_{\sigma_2, \dots, \sigma_N} \int d^3r_2 \dots d^3r_N \Psi^*(\mathbf{r}\sigma, \mathbf{r}\sigma_2, \dots, \mathbf{r}_N\sigma_N) \Psi(\mathbf{r}\sigma, \mathbf{r}\sigma_2, \dots, \mathbf{r}_N\sigma_N). \quad (2-4)$$

and the diagonal of second order spin-less electron matrix is

$$\rho_2(\mathbf{r}, \mathbf{r}) = N(N-1) \sum_{\sigma_1, \dots, \sigma_N} \int d^3r_3 \dots d^3r_N |\Psi(\mathbf{r}\sigma_1, \mathbf{r}\sigma_2, \dots, \mathbf{r}_N\sigma_N)|^2, \quad (2-5)$$

The electron spin density  $n_\sigma(\mathbf{r})$  defined as the average number of electrons at position  $\mathbf{r}$  with spin  $\sigma$  can be expressed as the diagonal of first order density matrix

$$\begin{aligned} n_\sigma(\mathbf{r}) &= \rho_1(\mathbf{r}\sigma, \mathbf{r}\sigma) \\ &= N \sum_{\sigma_2, \dots, \sigma_N} \int d^3r_2 \dots d^3r_N |\Psi(\mathbf{r}\sigma, \mathbf{r}\sigma_2, \dots, \mathbf{r}_N\sigma_N)|^2. \end{aligned} \quad (2-6)$$

Equation (2-1) and (2-6) gives

$$\sum_{\sigma} \int d^3r n_\sigma(\mathbf{r}) = N, \quad (2-7)$$

which is equal to the total number of the electrons in the system.

The expectation value of kinetic energy, Hartree energy and the external potential can be expressed as density matrices or density defined above

$$\langle \hat{T} \rangle = -\frac{1}{2} \sum_{\sigma} d^3r \frac{\partial}{\partial \mathbf{r}} \cdot \frac{\partial}{\partial \mathbf{r}} \rho_1(\mathbf{r} \sigma, \mathbf{r} \sigma) \Big|_{\mathbf{r}=\mathbf{r}, \sigma=\sigma}, \quad (2-8)$$

$$\langle \hat{V}_{ee} \rangle = \frac{1}{2} \int d^3r \int d^3r' \frac{\rho_2(\mathbf{r}, \mathbf{r}')}{|\mathbf{r} - \mathbf{r}'|}, \quad (2-9)$$

and

$$\langle \hat{V}_{ext} \rangle = \langle \Psi | \sum_i^N v(\mathbf{r}_i) | \Psi \rangle = \int d^3r n(\mathbf{r}) v(\mathbf{r}), \quad (2-10)$$

where  $n(\mathbf{r})$  is sum of the spin-up and spin-down density in (2-3) and the  $v(\mathbf{r})$  is external field.

### 2.1.2 Schrödinger Equation and Wavefunction Variational Principle

The wavefunction of electrons can be obtained by solving from the Schrödinger equation

$$\hat{H} \Psi(\mathbf{r}_1 \sigma_1, \dots, \mathbf{r}_N \sigma_N) = E \Psi(\mathbf{r}_1 \sigma_1, \dots, \mathbf{r}_N \sigma_N), \quad (2-11)$$

where  $\hat{H}$  is defined in (1-3),  $E$  is ground state energy and  $\Psi(\mathbf{r}_1 \sigma_1, \dots, \mathbf{r}_N \sigma_N)$  is ground state wavefunction. The ground-state energy and wavefunction are found by minimizing the expression  $\langle \Psi | \hat{H} | \Psi \rangle$ , where  $\Psi$  satisfies the normalization constraints (2-1).

Also, at the minima state, it satisfies the wavefunction variational principle:

$$\delta \{ \langle \Psi | \hat{H} | \Psi \rangle - \mu \langle \Psi | \Psi \rangle \} = 0, \quad (2-12)$$

where  $\mu$  is the Lagrange multiplier, and  $\langle \Psi | \Psi \rangle = 1$ . The minimization can be realized by the Rayleigh-Ritz method, which yields solutions in a restricted space of wavefunction by searching the extrema or the minimum when the analytical form for the true solution of (2-11) is intractable.

The Hamiltonian is invariant for a system, so (2-12) is

$$\langle \delta\Psi | \hat{H} - \mu | \Psi \rangle + c. c. = 0. \quad (2-13)$$

Since  $\delta\Psi$  is an arbitrary variation, it is equal to the Schrodinger equation (2-11). The solved Lagrange multiplier is ground-state energy  $E$ . The Wavefunction variational principle implies the Hellmann-Feynman theorems and the Hohenberg-Kohn [9] density functional variational principle that will be presented later.

### 2.1.3 Non-interacting System and Slater Determinant

In practice, solving the many-body Schrödinger equation is extremely difficult because of the electron-electron interaction. Since the electrons are identical particles, each electron can be equally treated as a particle under the same potential. The many-body interactions between electron-electron then are absorbed into identical potential for each electron. This is the idea of Hartree-Fock approach and Kohn-Sham approach which we will discuss later.

First, we can consider the simplest case: one electron system. The Hamiltonian of one electron in the presence of an external potential  $v(\mathbf{r})$  is

$$\hat{h} = -\frac{1}{2} \nabla^2 + v(\mathbf{r}). \quad (2-14)$$

The eigenstates and eigenvalues of the electron can be solved out from the one particle Schrödinger equation

$$\hat{h}\psi_{\alpha}(\mathbf{r}, \sigma) = \epsilon_{\alpha}\psi_{\alpha}(\mathbf{r}, \sigma). \quad (2-15)$$

Then, for a special case, the Hamiltonian for  $N$  non-interacting electrons is

$$\hat{H}_{non} = \sum_{i=1}^N \left[ -\frac{1}{2} \nabla_i^2 + v(\mathbf{r}_i) \right], \quad (2-16)$$

where  $v(\mathbf{r}_i)$  is the effective potential acting on each electron at position  $\mathbf{r}_i$ . The Schrödinger equation is

$$\hat{H}_{non}\Phi = E_{non}\Phi. \quad (2-17)$$

Because there is no spin-orbital interaction, the wavefunction  $\Phi$  can be constructed by the eigenfunctions of the one-electron problem of Eq. (2-14) and (2-15) and written as a Slater determinant

$$\Phi = \frac{1}{\sqrt{N!}} \begin{vmatrix} \psi_{\alpha_1}(\mathbf{r}_1, \sigma_1) & \psi_{\alpha_1}(\mathbf{r}_2, \sigma_2) & \cdots & \psi_{\alpha_1}(\mathbf{r}_N, \sigma_N) \\ \vdots & \vdots & \ddots & \vdots \\ \psi_{\alpha_N}(\mathbf{r}_1, \sigma_1) & \psi_{\alpha_N}(\mathbf{r}_2, \sigma_2) & \cdots & \psi_{\alpha_N}(\mathbf{r}_N, \sigma_N) \end{vmatrix}. \quad (2-18)$$

where  $\psi_{\alpha}(\mathbf{r}, \sigma)$  are  $N$  lowest energy state solved from the one electron system.

The total energy of the non-interacting system is

$$E_{non} = \epsilon_{\alpha_1} + \epsilon_{\alpha_2} + \cdots + \epsilon_{\alpha_N}, \quad (2-19)$$

and the density is given by the sum of  $|\psi_{\alpha_i}(\mathbf{r}, \sigma)|^2$ . Notice that the total energy of Hartree-Fock or Kohn-Sham method is not simply the sum of the  $N$  lowest eigenenergies, because they are not real non-interacting system and we will discuss it later. The Slater determinant satisfies the antisymmetric condition under exchange of any two electrons and satisfies the Pauli principle that if any  $\alpha_i$  equals any  $\alpha_j$  in Eq. (2-18), then  $\Phi = 0$ . If

several different Slater determinants yield the same non-interacting energy  $E_{non}$ , then a linear combination of them will be another antisymmetric eigenstate of  $\hat{H}_{non}$ .

Hartree-Fock approach uses Slater determinant (2-18) as wavefunction to construct the total energy

$$\begin{aligned} \langle \Phi | \hat{H} | \Phi \rangle = & \sum_i \int d^3r \psi_i^*(\mathbf{r}, \sigma) \left[ -\frac{1}{2} \nabla^2 + v_{ext}(\mathbf{r}) \right] \psi_i(\mathbf{r}, \sigma) \\ & + \frac{1}{2} \sum_{i,j} \int d^3r d^3r' \psi_j^*(\mathbf{r}, \sigma) \psi_i^*(\mathbf{r}', \sigma) \frac{1}{|\mathbf{r} - \mathbf{r}'|} \psi_j(\mathbf{r}, \sigma) \psi_i(\mathbf{r}', \sigma) \\ & - \frac{1}{2} \sum_{i,j} \int d^3r d^3r' \psi_j^*(\mathbf{r}, \sigma) \psi_i^*(\mathbf{r}', \sigma) \frac{1}{|\mathbf{r} - \mathbf{r}'|} \psi_j(\mathbf{r}', \sigma) \psi_i(\mathbf{r}, \sigma), \quad (2-20) \end{aligned}$$

where the second term is the Hartree energy and the third term is the exchange energy. However, a Slater determinant or a linear combination of a few Slater determinants could not describe the true wavefunction of electrons. Hartree-Fock method neglects the correlation of the orbitals, which could be important when the interactions between the electrons are strong. The Kohn-Sham approach is also a Hartree-Fock like method, which solves the non-interacting system. The effective potential of Kohn-Sham approach includes not only the exchange potential, but also the correlation potential in approximation.

#### 2.1.4 Hellmann-Feynman Theorem

If a Hamiltonian  $\hat{H}_\lambda$  depends upon a continuous parameter  $\lambda$ , then the wavefunction  $\Psi_\lambda$  and the ground-state energy  $E_\lambda$  of the Hamiltonian should depend implicitly on the parameter  $\lambda$ . The expectation value of ground-state energy is

$$E_\lambda = \langle \Psi_\lambda | \hat{H}_\lambda | \Psi_\lambda \rangle. \quad (2-21)$$

To study how the energy  $E_\lambda$  depends upon  $\lambda$ , we can make the partial derivative of the ground-state energy with respect to  $\lambda$

$$\begin{aligned} \frac{dE_\lambda}{d\lambda} &= \frac{d}{d\lambda} \langle \Psi_\lambda | \hat{H}_\lambda | \Psi_\lambda \rangle \Big|_{\lambda=\lambda} + \langle \Psi_\lambda | \frac{\partial \hat{H}_\lambda}{\partial \lambda} | \Psi_\lambda \rangle \\ &= E_\lambda \frac{d}{d\lambda} \langle \Psi_\lambda | \Psi_\lambda \rangle + \langle \Psi_\lambda | \frac{\partial \hat{H}_\lambda}{\partial \lambda} | \Psi_\lambda \rangle \end{aligned} \quad (2-22)$$

Because the wavefunction  $\Psi_\lambda$  satisfies **(2-1)** and  $\frac{d}{d\lambda} \langle \Psi_\lambda | \Psi_\lambda \rangle = 0$ , we have the Hellmann-Feynman theorem

$$\frac{dE_\lambda}{d\lambda} = \langle \Psi_\lambda | \frac{\partial \hat{H}_\lambda}{\partial \lambda} | \Psi_\lambda \rangle. \quad (2-23)$$

Equation **(2-23)** will be useful later for our understanding of  $E_{xc}$  and the electrostatic force acting on one nucleus within the Born-Oppenheimer approximation.

## 2.2 Definition of DFT

### 2.2.1 Hohenberg-Kohn Theorem and Constrained Search

The density of electrons has far fewer arguments than the wavefunction of electrons. Using a density functional to describe a many-body system instead of a wavefunction functional makes the computation much easier and more realizable. The existence of density functionals is based upon two theorems that were first proved by Hohenberg and Kohn [9]. Their approach is to formulate density functional theory as an exact theory of many-body systems that have the Hamiltonian written as **(1-3)**.

The first Hohenberg-Kohn theorem legitimizes the use of electron density  $n(\mathbf{r})$  as basic variable: For any system of interacting particles in an external potential  $v(\mathbf{r})$ , the potential  $v(\mathbf{r})$  is determined uniquely, except for a constant, by the ground-state particle density  $n(\mathbf{r})$ .

The second Hohenberg-Kohn theorem provides the energy variational principle: A universal functional for the energy  $E[n]$  in terms of density  $n(\mathbf{r})$  can be defined, valid for any external potential  $v(\mathbf{r})$ . For any particular  $v(\mathbf{r})$ , the exact ground-state energy of the system is the global minimum value of this functional, and the density  $n(\mathbf{r})$  that minimizes the functional is the exact ground-state density.

The following is an alternative approach of Levy constrained search [13], which is more general, simpler, and more constructive.

From the definition, the ground-state energy can be found by minimizing  $\langle \Psi | \hat{H} | \Psi \rangle$  over all normalized, antisymmetric  $N$ -particle wavefunctions:

$$E = \min_{\Psi} \langle \Psi | \hat{H} | \Psi \rangle . \quad (2-24)$$

The minimization procedure of (2-24) can be divided into two steps:

$$\begin{aligned} E &= \min_n \left( \min_{\Psi \rightarrow n} \langle \Psi | \hat{H} | \Psi \rangle \right) \\ &= \min_n \left( \min_{\Psi \rightarrow n} \langle \Psi | \hat{T} + \hat{V}_{ee} | \Psi \rangle + \int d^3r v(\mathbf{r}) n(\mathbf{r}) \right) . \end{aligned} \quad (2-25)$$

The first step is within the bracket of (2-25) to search the wavefunction  $\Psi$  in a restricted space, which yields a given density  $n(\mathbf{r})$  and minimizes expectation of Hamiltonian. We can notice the last term is potential energy due to the external field  $v(\mathbf{r})$ . From (2-10), we know all wavefunctions that yield the same  $n(\mathbf{r})$  also yield the same  $\langle \Psi | \hat{V}_{ext} | \Psi \rangle$ . The

second step is to minimize the energy by searing all  $n(\mathbf{r})$ . We can define the first term within the bracket of (2-25) in the second line as a universal functional

$$F[n] = \min_{\Psi \rightarrow n} \langle \Psi | \hat{T} + \hat{V}_{ee} | \Psi \rangle = \langle \Psi_n^{min} | \hat{T} + \hat{V}_{ee} | \Psi_n^{min} \rangle, \quad (2-26)$$

where  $\Psi_n^{min}$  is the wavefunction that yields the given density  $n(\mathbf{r})$  and minimizes  $\langle \Psi | \hat{T} + \hat{V}_{ee} | \Psi \rangle$ . So the ground state energy is

$$E = \min_n E[n] = \min_n \left\{ F[n] + \int d^3r v(\mathbf{r}) n(\mathbf{r}) \right\}, \quad (2-27)$$

which is a density functional.

The ground-state electron density must satisfy the variational principle

$$\delta \left\{ E[n] - \mu \left( \int d^3r n(\mathbf{r}) - N \right) \right\} = 0, \quad (2-28)$$

that yields the Euler-Lagrange equation

$$\mu = \frac{\delta E[n]}{\delta n(\mathbf{r})} = \frac{\delta F[n]}{\delta n(\mathbf{r})} + v(\mathbf{r}) \quad (2-29)$$

$\mu$  is a Lagrange multiplier, which can be adjusted until  $\int d^3r n(\mathbf{r}) = N$ .  $\delta F[n]/\delta n(\mathbf{r})$  is functional of electron density. So the external potential  $v(\mathbf{r})$  is uniquely determined by the electron density.

### 2.2.2 Kohn-Sham Non-interacting System

For a non-interacting  $N$ -electron system, Hamiltonian can be written as (2-16).

Without  $\hat{V}_{ee}$ , the equation (2-26) reduces to

$$F[n] = T_s[n] = \min_{\Psi \rightarrow n} \langle \Psi | \hat{T} | \Psi \rangle = \langle \Phi_n^{min} | \hat{T} | \Phi_n^{min} \rangle. \quad (2-30)$$



The minimizing wavefunction  $\Phi_n^{min}$  for a given density of non-interacting system should be a Slater determinant given by (2-18) or a linear combination of a few degenerate Slater determinants. And equation (2-29) reduces to

$$\mu_s = \frac{\delta T_s}{\delta n(\mathbf{r})} + v_s(\mathbf{r}). \quad (2-31)$$

In (2-31), the Kohn-Sham potential  $v_s(\mathbf{r})$  is a functional of  $n(\mathbf{r})$ . By absorbing the difference between  $\mu$  and  $\mu_s$  into  $v_s(\mathbf{r})$ , the chemical potential  $\mu$  for interacting system and non-interacting system of the same density are same. Here we assume the density  $n(\mathbf{r})$  can be solved from the interacting and non-interacting system.

The exchange-correlation energy  $E_{xc}[n]$  can be defined as

$$E_{xc}[n] = F[n] - T_s[n] - U[n], \quad (2-32)$$

where  $U[n]$  is Hartree energy

$$U[n] = \frac{1}{2} \int d^3r \int d^3r' \frac{n(\mathbf{r})n(\mathbf{r}')}{|\mathbf{r} - \mathbf{r}'|}. \quad (2-33)$$

The Euler-Lagrange equations (2-29) and (2-31) are consistent with one another if and only if

$$v_s(\mathbf{r}) = v(\mathbf{r}) + \frac{\delta U[n]}{\delta n(\mathbf{r})} + \frac{\delta E_{xc}[n]}{\delta n(\mathbf{r})} \quad (2-34)$$

Thus the Kohn-Sham method has the same Hamiltonian as that of many-body system (1-3), but has the non-interacting form

$$\hat{H}_s = \sum_{i=1}^N \left[ -\frac{1}{2} \nabla_i^2 + v_s(\mathbf{r}_i) \right]. \quad (2-35)$$

The Kohn-Sham method treats  $T_s[n]$  exactly for a given density, and leaves only  $E_{xc}[n]$  to be approximated. By solving the self-consistent one-electron like Schrödinger equation

$$\left[-\frac{1}{2}\nabla^2 + v_s(\mathbf{r})\right]\psi_\alpha(\mathbf{r}, \sigma) = \epsilon_\alpha \psi_\alpha(\mathbf{r}, \sigma), \quad (2-36)$$

the ground-state electron density distribution is given in term of the auxiliary Kohn-Sham orbitals,  $\psi_\alpha(\mathbf{r})$ :

$$n(\mathbf{r}) = \sum_{\alpha} \theta(\mu - \epsilon_{\alpha}) \psi_{\alpha}^*(\mathbf{r}) \psi_{\alpha}(\mathbf{r}). \quad (2-37)$$

The total energy of the system is not the sum of all eigenenergies (2-19), because  $v_s(\mathbf{r})$  is not a true external potential. The total energy can be written as

$$E = \sum_{\alpha} \theta(\mu - \epsilon_{\alpha}) \epsilon_{\alpha} - U[n] - \int d^3r n[\mathbf{r}] v_{xc}([n], \mathbf{r}) + E_{xc}[n], \quad (2-38)$$

where

$$v_{xc}([n], \mathbf{r}) = \frac{\delta E_{xc}[n]}{\delta n(\mathbf{r})}, \quad (2-39)$$

is the exchange-correlation potential. The flowchart of the self-consistent loop for solving K-S equation is given in Fig. 1.

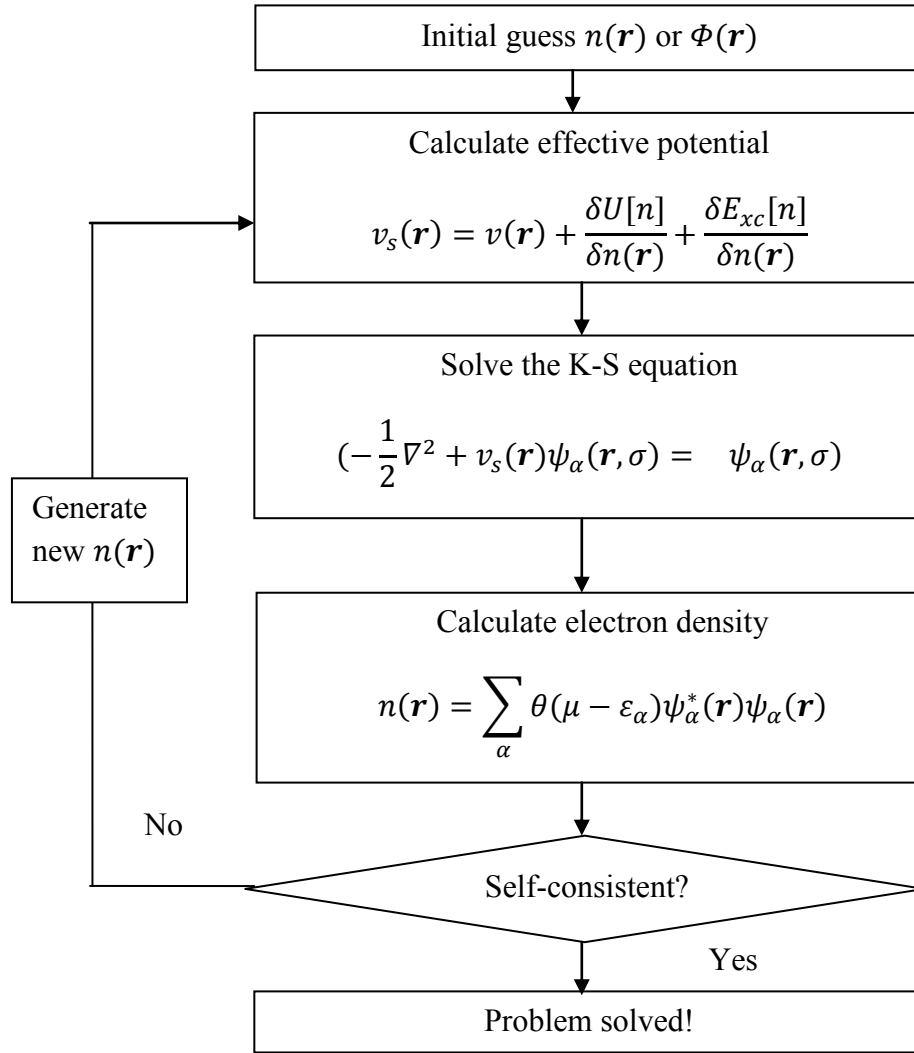


Fig. 1 The self-consistent loop for solving K-S equation

### 2.2.3 Exchange Energy and Correlation Energy

$E_{xc}[n]$  is defined in (2-32). It can be written as the sum of exchange and correlation terms:

$$E_{xc}[n] = E_x[n] + E_c[n] . \quad (2-40)$$

The exchange energy is defined as

$$E_x[n] = \langle \Phi_n^{min} | \hat{V}_{ee} | \Phi_n^{min} \rangle - U[n], \quad (2-41)$$

$\Phi_n^{min}$  is different from Hartree-Fock wavefunction, so the exchange energy defined here is different from Hartree-Fock exchange energy and so the kinetic energy. We note that

$$\begin{aligned} \langle \Phi_n^{min} | \hat{T} + \hat{V}_{ee} | \Phi_n^{min} \rangle &= \langle \Phi_n^{min} | \hat{T} | \Phi_n^{min} \rangle + \langle \Phi_n^{min} | \hat{V}_{ee} | \Phi_n^{min} \rangle \\ &= T_s[n] + U[n] + E_x[n] . \end{aligned} \quad (2-42)$$

In one-electron limit,  $\hat{V}_{ee}=0$ , so

$$E_x[n] = -U[n] \quad (N = 1) . \quad (2-43)$$

The exchange energy cancels the spurious Hartree energy completely.

From (2-32) and (2-40), we get the correlation energy

$$\begin{aligned} E_c[n] &= F[n] - \{T_s[n] + U[n] + E_x[n]\} \\ &= \langle \Psi_n^{min} | \hat{T} + \hat{V}_{ee} | \Psi_n^{min} \rangle - \langle \Phi_n^{min} | \hat{T} + \hat{V}_{ee} | \Phi_n^{min} \rangle \\ &= T_c + V_c , \end{aligned} \quad (2-44)$$

where  $T_c$  is  $\langle \Psi_n^{min} | \hat{T} | \Psi_n^{min} \rangle - \langle \Phi_n^{min} | \hat{T} | \Phi_n^{min} \rangle$  and  $V_c$  is  $\langle \Psi_n^{min} | \hat{V}_{ee} | \Psi_n^{min} \rangle - \langle \Phi_n^{min} | \hat{V}_{ee} | \Phi_n^{min} \rangle$ .  $E_c[n]$  is negative since  $\Psi_n^{min}$  is the wavefunction that yields density  $n$  and minimizes  $\langle \hat{T} + \hat{V}_{ee} \rangle$ , and  $T_c$  is positive since  $\Phi_n^{min}$  is the wavefunction that yields density  $n$  and minimizes  $\langle \hat{T} \rangle$ . So the potential energy piece  $V_c$  is negative because of  $V_c = E_c - T_c$  from (2-44). For one-electron limit

$$E_c[n] = 0 \quad (N = 1). \quad (2-45)$$

### 2.2.4 Coupling-constant Integration and Exchange-correlation Hole

The definitions of the exchange and correlation energies in (2-41) and (2-44) are formal ones, but provide no guidance for constructing these functionals. The correlation energy in (2-44) involves the real wavefunction  $\Psi_n^{min}$  that is hard to calculate for many-electron system. In practice, the coupling-constant integration [14, 15] and exchange-correlation hole can provide physical insight for construction them.

Consider a functional of density

$$F_\lambda[n] = \min_{\Psi \rightarrow n} \langle \Psi | \hat{T} + \lambda \hat{V}_{ee} | \Psi \rangle = \langle \Psi_n^{\min, \lambda} | \hat{T} + \lambda \hat{V}_{ee} | \Psi_n^{\min, \lambda} \rangle, \quad (2-46)$$

where  $\Psi_n^{\min, \lambda}$  is the functional that yields density  $n(\mathbf{r})$  and minimizes  $\langle \hat{T} + \lambda \hat{V}_{ee} \rangle$  and  $\lambda$  is a non-negative coupling constant. When  $\lambda = 1$ ,  $\Psi_n^{\min, \lambda}$  is  $\Psi_n^{\min}$ , the true interacting correlated ground-state wavefunction for density  $n$ . When  $\lambda = 0$ ,  $\Psi_n^{\min, \lambda}$  is  $\Phi_n^{\min}$ , the non-interacting or Kohn-Sham wavefunction for the same density  $n$ . We normally assume  $\lambda$  is a smooth variable that “adiabatic connection” any strength of the electron-electron interaction system between interacting system and non-interacting system. There is no physical meaning for intermediate values of  $\lambda$ .

From equations (2-32) and (2-26), the exchange-correlation energy can be expressed as

$$\begin{aligned} E_{xc}[n] \\ = \langle \Psi_n^{\min} | \hat{T} + \hat{V}_{ee} | \Psi_n^{\min} \rangle - \langle \Phi_n^{\min} | \hat{T} | \Phi_n^{\min} \rangle - U[n] \end{aligned}$$

$$\begin{aligned}
&= \langle \Psi_n^{\min, \lambda} | \hat{T} + \hat{V}_{ee} | \Psi_n^{\min, \lambda} \rangle_{=1} - \langle \Psi_n^{\min, \lambda} | \hat{T} + \hat{V}_{ee} | \Psi_n^{\min, \lambda} \rangle_{=0} - U[n] \\
&= \int_0^1 d\lambda \frac{d}{d\lambda} \langle \Psi_n^{\min, \lambda} | \hat{T} + \hat{V}_{ee} | \Psi_n^{\min, \lambda} \rangle - U[n].
\end{aligned} \tag{2-47}$$

Via Hellmann-Feynman theorem **(2-23)**, the coupling-constant integration [14, 15] of  $E_{xc}[n]$  can be expressed as:

$$E_{xc}[n] = \int_0^1 d\lambda \langle \Psi_n^{\min, \lambda} | \hat{V}_{ee} | \Psi_n^{\min, \lambda} \rangle - U[n]. \tag{2-48}$$

The exchange-correlation energy has the form of potential energy. The kinetic energy contribution to  $E_c$  has been subsumed by the coupling-correlation integration.

From **(2-9)**, the potential energy can be written as the form of second-order density matrix **(2-5)**. So the coupling-constant integration in **(2-48)** can be expressed as

$$\begin{aligned}
&\int_0^1 d\lambda \langle \Psi_n^{\min, \lambda} | \hat{V}_{ee} | \Psi_n^{\min, \lambda} \rangle \\
&= \int_0^1 d\lambda \frac{1}{2} \int d^3r \int d^3r' \frac{\rho_2^\lambda(\mathbf{r}, \mathbf{r}')}{|\mathbf{r} - \mathbf{r}'|} \\
&= \frac{1}{2} \int d^3r \int d^3r' \frac{\bar{\rho}_2(\mathbf{r}, \mathbf{r}')}{|\mathbf{r} - \mathbf{r}'|}.
\end{aligned} \tag{2-49}$$

The second-order density matrix  $\rho_2^\lambda(\mathbf{r}, \mathbf{r}')$  depends on the coupling constant  $\lambda$ .  $\rho_2(\mathbf{r}, \mathbf{r}')$  can be explained as the joint probability density of finding an electron at  $\mathbf{r}$ , and an electron at  $\mathbf{r}'$ . By standard probability theory, this is the product of the probability density of finding an electron at  $\mathbf{r}$  ( $n(\mathbf{r})$ ) and the conditional probability density of finding an electron at  $\mathbf{r}'$ , given that there is one at  $\mathbf{r}$  ( $n_2(\mathbf{r}, \mathbf{r}')$ ) [16]:

$$\rho_2(\mathbf{r}, \mathbf{r}') = n(\mathbf{r})n_2(\mathbf{r}, \mathbf{r}') = n(\mathbf{r})[n(\mathbf{r}') + n_{xc}(\mathbf{r}, \mathbf{r}')]. \tag{2-50}$$

The conditional density  $n_2(\mathbf{r}, \mathbf{r})$  can be thought as the average density of electrons at  $\mathbf{r}$ , given that there is an electron at  $\mathbf{r}$ . It can be written as the sum of the density  $n(\mathbf{r})$  at  $\mathbf{r}$  and the exchange-correlation-hole density  $n_{xc}(\mathbf{r}, \mathbf{r})$  at  $\mathbf{r}$  about an electron at  $\mathbf{r}$ . From equations (2-5), (2-6) and (2-50), we have

$$\int d^3r n_2(\mathbf{r}, \mathbf{r}) = N - 1, \quad (2-51)$$

and

$$\int d^3r n_{xc}(\mathbf{r}, \mathbf{r}) = -1. \quad (2-52)$$

The (2-52) can be explained as that if an electron is definitely at  $\mathbf{r}$ , it is missing from the rest of the system.

So (2-49) can be written as

$$\begin{aligned} & \frac{1}{2} \int d^3r \int d^3r' \frac{\bar{\rho}_2(\mathbf{r}, \mathbf{r}')}{|\mathbf{r} - \mathbf{r}'|} \\ &= \frac{1}{2} \int d^3r \int d^3r' \frac{n(\mathbf{r})[n(\mathbf{r}') + \bar{n}_{xc}(\mathbf{r}, \mathbf{r}')] }{|\mathbf{r} - \mathbf{r}'|} \\ &= U[n] + \frac{1}{2} \int d^3r \int d^3r' \frac{n(\mathbf{r})\bar{n}_{xc}(\mathbf{r}, \mathbf{r}')}{|\mathbf{r} - \mathbf{r}'|}. \end{aligned} \quad (2-53)$$

We note that for different values  $\lambda$ , the wavefunctions  $\psi_n^{\text{min}, \lambda}$  yield the same density  $n(\mathbf{r})$  but have different  $n_{xc}^\lambda(\mathbf{r}, \mathbf{r}')$ . The coupling-constant-averaged exchange-correlation hole density is

$$\bar{n}_{xc}(\mathbf{r}, \mathbf{r}') = \int_0^1 d\lambda n_{xc}^\lambda(\mathbf{r}, \mathbf{r}'). \quad (2-54)$$

So from (2-48) and (2-53), the exchange-correlation energy can be rewritten as:

$$E_{xc}[n] = \frac{1}{2} \int d^3r \int d^3r' \frac{n(\mathbf{r}) \bar{n}_{xc}(\mathbf{r}, \mathbf{r}')}{|\mathbf{r} - \mathbf{r}'|}, \quad (2-55)$$

which is just the electrostatic interaction between electron density and the coupling-constant-averaged exchange-correlation hole which surrounds it.

We can decompose  $\bar{n}_{xc}(\mathbf{r}, \mathbf{r}')$  into exchange hole density and correlation hole density. When  $\lambda = 0$ , it is non-interacting system and the exchange energy is the same as the third term in (2-20)

$$\begin{aligned} E_x &= -\frac{1}{2} \int d^3r \int d^3r' |\rho_1^{\lambda=0}(\mathbf{r}, \mathbf{r}')|^2 \\ &= \frac{1}{2} \int d^3r \int d^3r' \frac{n(\mathbf{r}) n_x(\mathbf{r}, \mathbf{r}')}{|\mathbf{r} - \mathbf{r}'|} \end{aligned} \quad (2-56)$$

where

$$\rho_1^{\lambda=0}(\mathbf{r}, \mathbf{r}') = \sum_{\alpha\sigma} (\mu - \varepsilon_{\alpha\sigma}) \psi_{\alpha}^*(\mathbf{r}, \sigma) \psi_{\alpha}(\mathbf{r}', \sigma) \quad (2-57)$$

So the exchange hole density is

$$n_x(\mathbf{r}, \mathbf{r}') = n_{xc}^{\lambda=0}(\mathbf{r}, \mathbf{r}') = -\frac{|\rho_1^{\lambda=0}(\mathbf{r}, \mathbf{r}')|^2}{n(\mathbf{r})} \quad (2-58)$$

Equation (2-58) shows

$$n_x(\mathbf{r}, \mathbf{r}') \leq 0, \quad (2-59)$$

so the exact exchange energy is negative. From (2-52) and (2-58), exchange hole has the constraint

$$\int d^3r' n_x(\mathbf{r}, \mathbf{r}') = -1. \quad (2-60)$$

Then the correlation hole can be defined as



$$n_c(\mathbf{r}, \mathbf{r}) = \bar{n}_{xc}(\mathbf{r}, \mathbf{r}) - n_x(\mathbf{r}, \mathbf{r}), \quad (2-61)$$

which satisfies the sum rule

$$\int d^3r n_c(\mathbf{r}, \mathbf{r}) = 0. \quad (2-62)$$

The correlation energy is from Coulomb repulsion, which tends to keep any two electrons apart in space and lower the total energy. That effect makes the hole deeper but more short-ranged, with a negative on-top correlation hole density:

$$n_c(\mathbf{r}, \mathbf{r}) \leq 0. \quad (2-63)$$

Because  $n_2(\mathbf{r}, \mathbf{r})$  is positive, so

$$\bar{n}_{xc}(\mathbf{r}, \mathbf{r}) \geq -n(\mathbf{r}) \quad (2-64)$$

which asserts that the hole cannot take away electrons that were not there initially. By the sum rule (2-62), there must be positive values of  $n_c(\mathbf{r}, \mathbf{r})$  that balance the negative contribution.

## 2.3 Semi-local Functionals

### 2.3.1 Uniform Electron Gas and LSDA

Uniform electron gas [6] is an important model in studying density functional theory because it is a simple system and the exchange energy can be analytically studied. It could be a physical system that is similar with the delocalized valence electrons in alkali metals. In this system, the electron density  $n(\mathbf{r})$  is uniform or constant over space, and the positive charges are uniformly distributed in the space to neutralize the negative

charge of electrons. We will first consider the spin-unpolarized electron gas of uniform density  $n$ . For exchange part, the spin-polarized case can be studied using spin scaling relations [17].

By translational symmetry, the Kohn-Sham potential  $v_s(\mathbf{r})$  must be uniform or constant and can be taken to be zero. The Kohn-Sham orbitals of uniform electron gas in a large cube of volume  $V = l^3$  with infinite potential well boundary have wavevector  $k_i = 2\pi n_i / l$ , where  $i$  can be  $x$  or  $y$  or  $z$  direction and  $n_i$  is a quantum number. If the volume is infinity ( $V \rightarrow \infty$ ), then the Kohn-Sham orbitals are plane waves  $\exp(i\mathbf{k} \cdot \mathbf{r})/\sqrt{V}$  with wavevectors  $\mathbf{k}$  and energies  $k^2/2$ , where  $k$  becomes a continuous value. The number of orbitals in a volume  $d^3k$  of wavevector space is  $2[V/(2\pi)^3]d^3k$  [18].

Let  $N = nV$  be the number of electrons in volume  $V$ , the number of electrons that occupy the  $N$  lowest Kohn-Sham spin orbitals is

$$N = 2 \sum_{\mathbf{k}} \theta(k_F - k) = 2 \frac{V}{(2\pi)^3} \int_0^{k_F} dk 4\pi k^2 = V \frac{k_F^3}{3\pi^2}, \quad (2-65)$$

where  $k_F$  is called the Fermi Wavevector, that represents the highest energy among all occupied orbitals. Then, the electron density is

$$n = \frac{k_F^3}{3\pi^2} = \frac{3}{4\pi r_s^3}, \quad (2-66)$$

where  $r_s$  is the radius of a sphere which on average contains one electron.

The kinetic energy of an orbital is  $k^2/2$ . Two electrons with different spins can have same wavevector. The average kinetic energy per electron is

$$t_s(n) = \frac{2}{N} \sum_k \theta(k_F - k) \frac{k^2}{2} = \frac{2V}{N(2\pi)^3} \int_0^{k_F} dk 4\pi k^2 \frac{k^2}{2} = \frac{3}{5} \frac{k_F^2}{2}, \quad (2-67)$$

or 3/5 of the Fermi energy. The kinetic energy from uniform electron gas is also known as the Thomas-Fermi kinetic-energy approximation. From (2-66) the average kinetic energy can be written in terms of  $n$  or  $r_s$ :

$$t_s(n) = \frac{3}{10} (3\pi^2 n)^{2/3} = \frac{3}{10} \frac{(9\pi/4)^{2/3}}{r_s^2}. \quad (2-68)$$

All of this kinetic energy satisfies the Pauli exclusion principle that no more two identical electrons occupy the same orbitals.

Using the same way, the exchange energy of the uniform electron can be calculated. We need the Kohn-Sham first order matrix for electrons defined in (2-57)

$$\begin{aligned} \rho_1^{\lambda=0}(\mathbf{r} + \mathbf{u}, \mathbf{r}) &= 2 \sum_k \theta(k_F - k) \frac{\exp(-i\mathbf{k} \cdot (\mathbf{r} + \mathbf{u}))}{\sqrt{V}} \frac{\exp(i\mathbf{k} \cdot \mathbf{r})}{\sqrt{V}} \\ &= \frac{2}{(2\pi)^3} \int_0^{k_F} dk 4\pi k^2 \int \frac{d\Omega_{\mathbf{k}}}{4\pi} \exp(-i\mathbf{k} \cdot \mathbf{u}) \\ &= \frac{1}{\pi^2} \int_0^{k_F} dk k^2 \frac{\sin(ku)}{ku} \\ &= \frac{k_F^3}{\pi^2} \frac{\sin(k_F u) - k_F u \cos(k_F u)}{(k_F u)^3} \end{aligned} \quad (2-69)$$

The exchange-hole density at distance  $u$  from an electron at  $\mathbf{r}$  is, by (2-58)

$$n_x(u) = - \frac{|\rho_1^{\lambda=0}(\mathbf{r} + \mathbf{u}, \mathbf{r})|^2}{n}, \quad (2-70)$$

exchange hole density is not positive, which could range from  $-n/2$  (at  $u = 0$ , one electron situation) to 0 ( $u \rightarrow \infty$ ). The exchange energy per electron is

$$\begin{aligned}
e_x^{unif}(n) &= \frac{1}{2N} \int d^3r \int d^3u \frac{\mathbf{n} \cdot \mathbf{n}_x(u)}{|\mathbf{u}|} \\
&= \int_0^\infty du 2\pi u n_x(u) = -\frac{3}{4\pi} k_F.
\end{aligned} \tag{2-71}$$

It also can be written in terms of  $n$  or  $r_s$ :

$$e_x^{unif}(n) = -\frac{3}{4\pi} (3\pi^2 n)^{1/3} = -\frac{3}{4\pi} \frac{(9\pi/4)^{1/3}}{r_s}. \tag{2-72}$$

The orbitals of uniform electron gas are orthogonal plane waves. For different  $i$  and  $j$  in third term of (2-20), the integral is zero. For  $i = j$ , the two orbitals are identical. So the exchange energy of uniform electron gas is due to the Pauli exclusion principle only.

Exact analytical expression for  $e_c(n)$ , the correlation energy per electron of the uniform gas, are known only in extreme limits. The high-density ( $r_s \rightarrow 0$ ) limit is also the weak-coupling limit, in which

$$e_c^{unif}(n) = c_0 \ln r_s - c_1 + \dots \quad (r_s \rightarrow 0) \tag{2-73}$$

from many-body perturbation theory [19]. The two positive constants  $c_0$  and  $c_1$  can be calculated [19, 20].

The low-density ( $r_s \rightarrow \infty$ ) limit is also the strong coupling limit [21], in which

$$e_c^{unif}(n) \rightarrow -\frac{d_0}{r_s} + \frac{d_1}{r_s^{3/2}} + \dots \quad (r_s \rightarrow \infty). \tag{2-74}$$

The constant  $d_0$  and  $d_1$  in (2-74) can be estimated from the Madelung electrostatic and zero-point vibrational energies of the Wigner crystal [8], respectively.

An expression which encompasses both limits (2-73) and (2-74) is [22]

$$e_c^{unif}(n) = -2c_0(1 + \alpha_1 r_s) \ln \left[ 1 + \frac{1}{2c_0(\beta_1 r_s^{1/2} + \beta_2 r_s + \beta_3 r_s^{3/2} + \beta_4 r_s^2)} \right], \quad (2-75)$$

where

$$\beta_1 = \frac{1}{2c_0} \exp\left(\frac{c_1}{2c_0}\right), \quad (2-76)$$

$$\beta_2 = 2c_0\beta_1^2. \quad (2-77)$$

The coefficients  $\alpha_1$ ,  $\beta_3$ , and  $\beta_4$  are found by fitting to accurate Quantum Monte Carlo correlation energies [7].

The local spin density approximation (LSDA) [10] for the exchange-correlation energy was proposed in the original work of Kohn and Sham, which uses spin density  $n_\uparrow$  and  $n_\downarrow$  :

$$E_{xc}^{LSDA}[n_\uparrow, n_\downarrow] = \int d^3r n(\mathbf{r}) e_{xc}^{unif}(n_\uparrow, n_\downarrow), \quad (2-78)$$

where  $e_{xc}^{unif}(n_\uparrow, n_\downarrow)$  is the exchange-correlation energy per electron for the uniform electron gas. The exchange part  $e_x^{unif}(n_\uparrow, n_\downarrow)$  of  $e_{xc}^{unif}(n_\uparrow, n_\downarrow)$  is analytical expression, that can be estimated from  $e_x^{unif}(n)$  of (2-72) with the spin-scaling relation [17]:

$$e_x^{unif}(n_\uparrow, n_\downarrow) = e_x^{unif}(n) \frac{[(1 + \zeta)^{4/3} + (1 - \zeta)^{4/3}]}{2}, \quad (2-79)$$

where,  $\zeta$  is spin polarization

$$\zeta = \frac{(n_\uparrow - n_\downarrow)}{(n_\uparrow + n_\downarrow)}. \quad (2-80)$$

The correlation part  $e_c^{unif}(n_\uparrow, n_\downarrow)$  of  $e_{xc}^{unif}(n_\uparrow, n_\downarrow)$  can be interpolated from  $e_c^{unif}(n_\uparrow = n/2, n_\downarrow = n/2)$  for spin-unpolarized uniform electron gas and  $e_c^{unif}(n_\uparrow = n, n_\downarrow = 0)$  for fully spin-polarized uniform electron gas, where  $e_c^{unif}(n_\uparrow = n/2, n_\downarrow = n/2)$  is provided in (2-75) and  $e_c^{unif}(n_\uparrow = n, n_\downarrow = 0)$  has the form of (2-75) but different fitted parameters. The correlation energy per electron for spin-polarized uniform electron gas is [23]

$$e_c^{unif}(n_\uparrow, n_\downarrow) = e_c^{unif}(n) + \alpha_c(n)\zeta^2 + O(\zeta^4) \quad (2-81)$$

where  $\alpha_c(n)$  is the correlation contribution to the spin stiffness that can be parameterized from (2-75).

### 2.3.2 Slowly Varying Density and (meta-) GGA Approximation

To study a more general system, which is not ideal uniform electron gas system, we can introduce the reduced density gradient

$$s = \frac{|\nabla n|}{2k_F n} = \frac{|\nabla n|}{2(3\pi^2)^{1/3} n^{4/3}} = \frac{3}{2} \left( \frac{4}{9\pi} \right)^{1/3} |\nabla r_s|, \quad (2-82)$$

with its square

$$p = s^2, \quad (2-83)$$

and the reduced Laplacian

$$q = \frac{\nabla^2 n}{4(3\pi^2)^{2/3} n^{5/3}}, \quad (2-84)$$

for the measurement of inhomogeneity. The reduce density gradient  $s$  measures how fast and how much the density varies on the scale of the local Fermi wavelength  $2\pi/k_F$ . The slowly varying system means that not only  $s$ , but also  $q$  is small.

For a slowly-varying spin-unpolarized density, the exact exchange energy has the fourth-order gradient expansion [24]

$$E_x[n] = \int d^3r n e_x^{unif}(n) \left[ 1 + \frac{10}{81} p + \frac{146}{2025} q^2 - \frac{73}{146} qp + Dp^2 + \dots \right] \quad (2-85)$$

where  $D \approx 0$ . For the expansion of stable exchange energy, the odd gradient terms are omitted.

The correlation energy has the second-order gradient expansion,

$$E_c[n] = \int d^3r n [e_c^{unif}(n_\uparrow, n_\downarrow) + C_c(n_\uparrow, n_\downarrow) \frac{|\nabla n|^2}{n^{4/3}} + \dots], \quad (2-86)$$

where  $C_c(n_\uparrow, n_\downarrow)$  is a known coefficient [25-27] and

$$C_c(n_\uparrow, n_\downarrow) = \frac{0.066725}{16\phi^2} \left(\frac{\pi}{3}\right)^{1/3} \quad (2-87)$$

in the high-density or weak-interaction limit [28]. Here

$$\phi(\zeta) = \frac{1}{2} [(1 + \zeta)^{2/3} + (1 - \zeta)^{2/3}] \quad (2-88)$$

and  $\zeta$  is the relative spin polarization of **(2-80)**.

The gradient expansion approximation (GEA) [10, 28] keeps the second order gradient terms of the expansion **(2-85)** and **(2-86)**, which might be expected to give a better description than LDA, but in practice it works worse. Langreth and Perdew gave the explanation of the failure of GEA that the correlation energy of the GEA is wrong at

small  $k$  using the expansion method [26], where  $k$  is the wavevector of dynamic density fluctuations. Later, Perdew explained the error of  $E_x$  of the GEA in the real space, where at large interelectron separation  $u$  the GEA is spurious [29]. So by cutting off the exchange-correlation hole in real space and restoring the sum rule on the correlation hole, Perdew and Wang gave a much better functional PW91 [30, 31]. Compared to the LSDA, the GGA [29] includes an additional semi-local information, the gradients of the spin densities, and can be written as

$$E_{xc}[n] = \int d^3r n e_{xc}^{unif}(n) F_{xc}(n_{\uparrow}, n_{\downarrow}, \nabla n_{\uparrow}, \nabla n_{\downarrow}) \quad (2-89)$$

where  $F_{xc}$  is the enhancement factor.

With the advent of GGA's [31-39], density functional theory has become popular not only in solid state physics, but also in quantum chemistry. e.g., the standard nonempirical Perdew-Burke- Ernzerhof (PBE) GGA [34, 40] predicts reasonable lattice constants, and improves atomization energies to about 10 kcal/mol, and the PBEsol [41], which has diminished gradient dependence designed specifically for solids and solid surfaces near equilibrium, predicts good lattice constant and surface energies.

Meta-GGA is a natural way to improve accuracy further by making use of more additional semi-local information, e.g., the Laplacian of the density  $\nabla^2 n_{\sigma}$  or the kinetic energy densities  $\tau_{\sigma}$ :

$$E_{xc}[n] = \int d^3r n e_{xc}^{unif}(n) F_{xc}(n_{\uparrow}, n_{\downarrow}, \nabla n_{\uparrow}, \nabla n_{\downarrow}, \nabla^2 n_{\uparrow}, \nabla^2 n_{\downarrow}, \tau_{\uparrow}, \tau_{\downarrow}), \quad (2-90)$$

where



$$\tau_{\sigma} = \sum_{\alpha}^{\text{occup}} \frac{1}{2} |\nabla \psi_{\alpha\sigma}(r)|^2 \quad (2-91)$$

is the kinetic energy density [42-48], and  $\nabla^2 n$  is Laplacian of the density [39, 49, 50].  $\tau$  can be used to recognize the one- and two-electron density regions. Moreover, it can make a correction to the exchange-correlation energy to fourth order in  $\nabla$  for slowly varying densities.

The TPSS meta-GGA [47] predicts lattice constants only a little smaller than those of PBE, but gives better atomization energies for molecules than PBE does [47, 51]. The revTPSS meta-GGA [48], which takes insights from the PBEsol [41] construction, gives lattice constants as accurate as those of PBEsol while keeping the atomization energies as accurate as those of TPSS [48]. We will discuss the performance for the lattice constants on 58 solids in Chapter 3. Some other new meta-GGAs outperforms better than PBE GGA in thorough chemical properties, which will be discussed in Chapter 4.

### 2.3.3 Beyond the Semi-local Functional

Perdew has proposed the notion of Jacob's ladder for exchange-correlation energy of density functional approximations [52]. Arising from the first rung of Jacob's ladder to higher levels, more constraints are added to construct the exchange-correlation energy. The top of the ladder reaches to the heaven of chemical accuracy. The first rung of Jacob's ladder is LSDA, which is the basic rung, using only  $n_{\uparrow}$  and  $n_{\downarrow}$ , the second rung GGA adds the ingredient  $\nabla n_{\uparrow}$  and  $\nabla n_{\downarrow}$ , and the third rung is meta-GGA, which adds  $\nabla^2 n_{\uparrow}$  and  $\nabla^2 n_{\downarrow}$ ,  $\tau_{\uparrow}$ , and  $\tau_{\downarrow}$ . Functionals that belong to the first three rungs are semi-local

functionals. Beyond the semi-local functionals, the ingredient of non-locality can be added. A fraction of exact exchange energy can be mixed with (meta-)GGA exchange and correlation energy [53, 54]:

$$E_{xc} = aE_x^{exact} + (1 - a)E_x^{GGA} + E_c^{GGA} \quad (2-92)$$

where the constant  $a$  can be fitted empirically. B3LYP [54, 55] is a type of hybrid functional, and we will discuss the performance of B3LYP in chapter 4.

On the fifth rung of the Jacob ladder, some partial exact correlation energy can be added. The random phase approximation (RPA) [26, 56, 57] is expected to work well for some van der Waals systems. Van der Waals is a difficult issue for semi-local functionals, because it is a long-range attraction between chemical species, arising from instantaneous charge fluctuations and involving information of non-locality, which is missed in semi-local functionals. However, from our study, we can see some semi-local functionals, e.g., M06L [44] and MGGA\_MS [58], can capture some van der Waals interactions. We also discuss that in Chapter 4.

## 2.4 Density Functional Perturbation Theory

### 2.4.1 Density Functional Perturbation Theory

As we discussed before, the Hamiltonian or the external potential can depend upon some parameters  $\lambda$ . The first order derivative of the ground-state energy with respect to one parameter can be read from Hellmann-Feynman theorem (2-23). And the second order derivative of the ground-state energy is

$$\frac{\partial^2 E}{\partial \lambda_i \partial \lambda_j} = \int d^3 r \frac{\partial n_\lambda(\mathbf{r})}{\partial \lambda_i} \frac{\partial v_\lambda(\mathbf{r})}{\partial \lambda_j} + \int d^3 r n(\mathbf{r}) \frac{\partial^2 v_\lambda(\mathbf{r})}{\partial \lambda_i \partial \lambda_j}. \quad (2-93)$$

The electron-density response,  $\partial n_\lambda(\mathbf{r})/\partial \lambda$  in (2-93) can be evaluated by linearizing the equation (2-37), one-electron Schrödinger equation (2-36) and the self-consistent Kohn-Sham potential (2-34). From (2-37), the density variation with respect to the wave function variation is

$$n(\mathbf{r}) = 2\text{Re} \sum_{\alpha} \theta(\mu - \varepsilon_{\alpha}) \psi_{\alpha}^*(\mathbf{r}) \psi_{\alpha}(\mathbf{r}). \quad (2-94)$$

To simplify the notation, the finite-difference operator  $\delta$  is used, which is defined as

$$F = \sum_i \frac{\partial F}{\partial \lambda_i} \delta \lambda_i. \quad (2-95)$$

The variation of the Kohn-Sham orbitals,  $\psi_{\alpha}(\mathbf{r})$ , is obtained by standard first-order perturbation theory [59]:

$$(\hat{h} - \varepsilon_{\alpha}) \delta \psi_{\alpha} = -(\delta v_s - \delta \varepsilon_{\alpha}) \psi_{\alpha}, \quad (2-96)$$

where

$$\hat{h} = -\frac{1}{2} \nabla^2 + v_s(\mathbf{r}_i) \quad (2-97)$$

is the unperturbed Kohn-Sham Hamiltonian, and

$$v_s(\mathbf{r}) = v(\mathbf{r}) + e^2 \int d\mathbf{r}' \frac{n(\mathbf{r}')}{|\mathbf{r} - \mathbf{r}'|} + \left. \frac{dv_{xc}(n)}{dn} \right|_{n=n(\mathbf{r})} n(\mathbf{r}) \quad (2-98)$$

is the first-order correction to the self-consistent potential that can be easily derived from (2-34).

The wavefunction variation can be expressed from the first-order perturbation theory:

$$\psi_\alpha(\mathbf{r}) = \sum_{\beta \neq \alpha} \psi_\beta(\mathbf{r}) \frac{\langle \psi_\beta | v_s | \psi_\alpha \rangle}{\varepsilon_\alpha - \varepsilon_\beta}, \quad (2-99)$$

where  $\beta$  is summed for all the state in the system, occupied and empty, with the exception of the state being considered. So the electron-density response, **(2-94)**, can be expressed as

$$n(\mathbf{r}) = 2 \sum_{\alpha=1} \sum_{\beta \neq \alpha} \psi_\alpha^*(\mathbf{r}) \psi_\beta(\mathbf{r}) \frac{\langle \psi_\beta | v_s | \psi_\alpha \rangle}{\varepsilon_\alpha - \varepsilon_\beta}. \quad (2-100)$$

In **(2-100)**, the contributions to the electron density response from products of occupied states cancel each other, so that the  $\beta$  index can be thought of as attaching to conduction states only. So to study density response, we can only calculate the wavefunction variation projected to the empty-state one. A projector  $P_c = \sum_\beta |\psi_\beta\rangle\langle\psi_\beta|$  onto the empty-state manifold can be used on both side of **(2-96)** to solve the variation of the Kohn-Sham orbitals

$$\left(-\frac{1}{2}\nabla^2 + v_s - \varepsilon_\alpha\right) P_c \Delta \psi_\alpha = -P_c \Delta v_s \psi_\alpha \quad (2-101)$$

In practice, instead of the full spectrum of Kohn-Sham orbitals, only occupied orbitals are used to construct the right hand side of **(2-101)**, and conjugate-gradient [60-62] or any other iterative method [60, 63] can used to solve the self-consistent linear system [64]. The flowchart of the self-consistent loop for solving the perturbation equation is given in Fig. 2

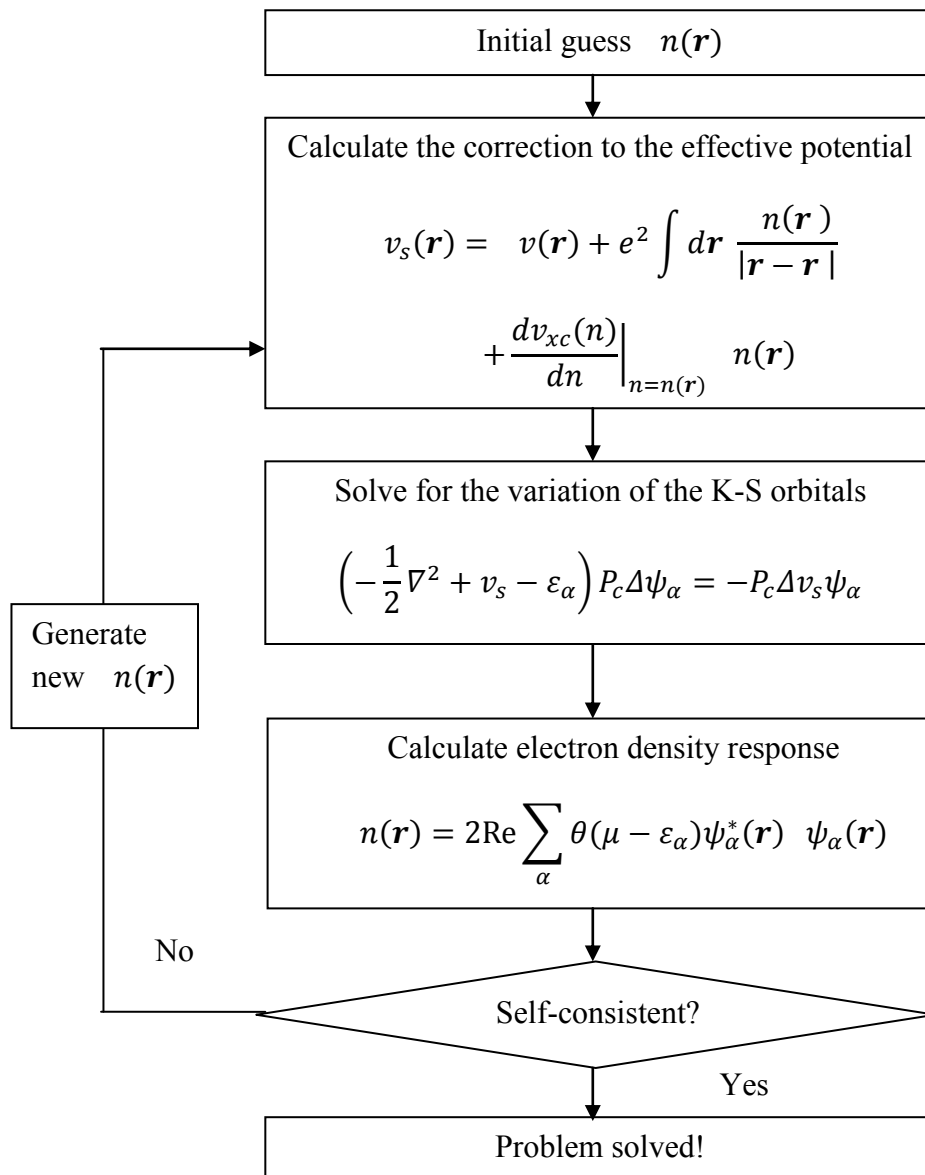


Fig. 2 The self-consistent loop for solving the linear perturbation equation

### 2.4.2 Lattice Dynamics from Electronic-Structure Theory

The equilibrium geometry of the system is given by the condition that the forces acting on individual nuclei vanish:

$$F_I \equiv -\frac{\partial E(\mathbf{R})}{\partial \mathbf{R}_I} = 0. \quad (2-102)$$

Within the Born-Oppenheimer approximation, nuclear coordinates act as parameters in the electronic Hamiltonian (1-1). From Hellmann-Feynman theorem (2-23),  $\lambda = \mathbf{R}$  and the force acting on the  $I$ -th nucleus in the electronic ground state is

$$F_I = \langle \Psi(\mathbf{R}) \left| -\frac{\partial \hat{H}(\mathbf{R})}{\partial \mathbf{R}_I} \right| \Psi(\mathbf{R}) \rangle, \quad (2-103)$$

where  $\Psi(\mathbf{R})$  is the electronic ground-state wave function of the Born-Oppenheimer Hamiltonian. This Hamiltonian depends on  $\mathbf{R}$  via the electron-ion interaction that couples to the electronic degrees of freedom only through the electron charge density. The Hellmann-Feynman theorem states in this case that

$$F_I = - \int d^3r n(\mathbf{r}) \frac{\partial v_R(\mathbf{r})}{\partial \mathbf{R}_I} - \frac{\partial E_N(\mathbf{R})}{\partial \mathbf{R}_I}, \quad (2-104)$$

where  $v_R(\mathbf{r})$  is the electron-nucleus interaction:

$$v_R(\mathbf{r}) = \sum_{i,I} \frac{Z_I e^2}{|\mathbf{r}_i - \mathbf{R}_I|}, \quad (2-105)$$

and  $E_N(\mathbf{R})$  is the electrostatic interaction between different nuclei:

$$E_N(\mathbf{R}) = \frac{1}{2} \sum_{I \neq J} \frac{Z_I Z_J e^2}{|\mathbf{R}_I - \mathbf{R}_J|}. \quad (2-106)$$

The vibrational frequencies of nuclei can be determined by the eigenvalues of the Hessian of the total energy, scaled by the nuclear masses:

$$\det \left| \frac{1}{\sqrt{M_I M_J}} \frac{\partial^2 E(\mathbf{R})}{\partial \mathbf{R}_I \partial \mathbf{R}_J} - \omega^2 \right| = 0. \quad (2-107)$$

We need to compute the Hessian of the energy surface, which is a matrix of second-order partial derivative of the total energy and is often called matrix of interatomic force constants. It can be obtained by differentiating the Hellmann-Feynman forces with respect to nuclear coordinates [65, 66],

$$\begin{aligned} \frac{\partial^2 E(\mathbf{R})}{\partial \mathbf{R}_I \partial \mathbf{R}_J} &\equiv - \frac{\partial \mathbf{F}_I}{\partial \mathbf{R}_J} \\ &= \int d^3r \frac{\partial n_{\mathbf{R}}(\mathbf{r})}{\partial \mathbf{R}_J} \frac{\partial v_{\mathbf{R}}(\mathbf{r})}{\partial \mathbf{R}_I} + \int d^3r n(\mathbf{r}) \frac{\partial^2 v_{\mathbf{R}}(\mathbf{r})}{\partial \mathbf{R}_I \partial \mathbf{R}_J} + \frac{\partial^2 E_N(\mathbf{R})}{\partial \mathbf{R}_I \partial \mathbf{R}_J}. \end{aligned} \quad (2-108)$$

Then calculation of Hessian turns out to be the calculations of the ground-state electron charge density  $n_{\mathbf{R}}(\mathbf{r})$  and its linear response to a distortion of the nuclear geometry,  $\partial n_{\mathbf{R}}(\mathbf{r})/\partial \mathbf{R}_J$ , which can be obtained from self-consistent equations (2-36), (2-37), and (2-101), (2-94), separately.

### 2.4.3 Vibrational States in Crystalline Solids

Within the Born-Oppenheimer adiabatic approximation the nuclei are fixed to position  $\mathbf{R}$ . The total energy can be expanded in a Taylor series respect to  $\mathbf{u}_I$  :

$$E(\mathbf{R}_I + \mathbf{u}_I) = E(\mathbf{R}_I) + \sum_I \frac{\partial E}{\partial \mathbf{u}_I} \mathbf{u}_I + \frac{1}{2} \sum_{I,J} \frac{\partial^2 E}{\partial \mathbf{u}_I \partial \mathbf{u}_J} \mathbf{u}_I \mathbf{u}_J + \dots, \quad (2-109)$$

where  $\mathbf{u}_I$  is the displacement of atom  $I$ . If the  $\mathbf{R}_I$  is the equilibrium position, then force acting on the atom  $I$  is:

$$\mathbf{M}_I \ddot{\mathbf{u}}_I = - \sum_J \frac{\partial^2 E}{\partial \mathbf{u}_I \partial \mathbf{u}_J} \mathbf{u}_J \quad (2-110)$$

We can search the solution in the form of a phonon, which is a periodic vibration in solid.

The displacement of an atom can be expanded as a lot of plane waves. For each vector  $\mathbf{q}$  in the first Brillouin zone, the plane wavefunction is

$$\mathbf{u}_{\mu S \alpha}(t) = \frac{1}{\sqrt{M_S}} \mathbf{u}_{S \alpha}(\mathbf{q}) e^{i(\mathbf{q} \mathbf{R}_\mu - \omega_{\mathbf{q}} t)}, \quad (2-111)$$

where the time dependence is given by a simple exponential  $e^{i\omega_{\mathbf{q}} t}$ .  $\alpha$  represents  $x$  or  $y$  or  $z$  direction and  $\mu$  indicates the displacement of the atoms  $S$  in each cell identified by the Bravais lattice  $\mathbf{R}_\mu$ .

Inserting this solution in the equations of (2-110) and writing  $I = (\mu, S)$ ,  $J = (\nu, S)$  we obtain an eigenvalue problem for  $3 \times N_{at}$  variables  $\mathbf{u}_{S \alpha}(\mathbf{q})$

$$\omega_{\mathbf{q}}^2 \mathbf{u}_{S \alpha}(\mathbf{q}) = \sum_{S \beta} D_{S \alpha S \beta}(\mathbf{q}) \mathbf{u}_{S \beta}(\mathbf{q}) \quad (2-112)$$

where

$$D_{S \alpha S \beta}(\mathbf{q}) = \frac{1}{\sqrt{M_S M_S}} \sum_{\nu} \frac{\partial^2 E}{\partial \mathbf{u}_{\mu S \alpha} \partial \mathbf{u}_{\nu S \beta}} e^{i \mathbf{q} (\mathbf{R}_\nu - \mathbf{R}_\mu)} \quad (2-113)$$

is called dynamical matrix of the solid. With  $\partial n / \partial \mathbf{u}$  for all the perturbations,  $D_{S \alpha S \beta}(\mathbf{q})$  can be calculated at any given  $\mathbf{q}$  points. Diagonalizing this matrix we can obtain frequencies  $\omega_{\mathbf{q}}$ .



## 2.5 Applying and Testing on Condensed Matter Physics and Quantum Chemistry

The developed density functional approximations can be built into some standard efficient codes. Those standard codes are widely used in quantum mechanical applications and help DFT to be popular. For example, for solids, there are plan-wave codes Vienna ab initio simulation package (VASP) [67-70] and Quantum Espresso (QE) [71] which use delocalized orbitals, or BAND-structure package [72-74], which uses localized orbital. For molecules, the Gaussian code is popular, which uses the localized Gaussian-type orbitals.

The number of proposed exchange-correlation functional approximations is immense but the exact functional is unknown. The calculation efficiency and accuracy depend on the choosing of different functionals. The high level functionals on Jacobs' ladder normally can give better description than lower level functionals, but it also demands more calculation resource. On another hand, for a functional, it can yield good results for some systems, but it does not work for all systems. It is still a challenge for developers to construct a general functional that more close to exact functional.

Semi-local functionals only use locality information, so the calculation is efficient. For condensed matter physics, semi-local functionals are popular, because they can give good results. The static lattice energy and the crystal vibration energy can be calculated from DFT and DFPT, which can be used to calculate the geometry structure. For molecules, the performance of DFT can be tested by benchmarking data sets, which can

give a statistic study for a functional. In the next two chapters, we will apply semi-local functionals to condensed matter physics and quantum chemistry.

## CHAPTER 3

# LATTICE CONSTANTS FROM SEMI-LOCAL DENSITY FUNCTIONALS WITH ZERO-POINT PHONON CORRECTION

This chapter was published as [75] “Lattice constants from semi-local density functionals with zero-point phonon correction”, P. Hao, Y. Fang, J. Sun, G. I. Csonka, P. H. T. Philipsen, and J. P. Perdew, *Physical Review B* **85**, 014111 (2012).

### 3.1 Introduction of Lattice Constant Calculation by Using First-Principle DFT with Zero-Point Energy Correction

The equilibrium lattice constant of a solid [18] can be measured accurately (e.g., by X-ray diffraction) at low temperature and extrapolated to absolute zero, where it becomes a fundamental ground-state property. All properties of a solid depend upon the lattice constant, and some—e.g., ferromagnetism, ferroelectricity or epitaxy—can be very sensitive to it. Kohn-Sham density functional theory [10] (DFT) in principle predicts the ground-state energy and density of electrons in the presence of a static external potential and has long been used to calculate the equation of state or energy per unit cell of a solid

as a function of the lattice constant for a given crystal structure. The equilibrium lattice constant is then the one that minimizes the energy. The accuracy of the predicted lattice constant is a test of the accuracy of the approximate density functional that must be employed for the exchange-correlation energy.

The simplest calculation of the lattice constant assumes a perfect static lattice. If the nuclei were fully classical particles, they would form such a lattice at zero temperature [76]. But in quantum mechanics all systems undergo fluctuation in their ground state. The nuclear fluctuation in a solid is crystal vibration and exists even at zero temperature. For a periodic solid, the vibration has normal modes which are quantized as phonons [18]. Although the zero-point energy of the vibration is minor compared to the kinetic energy of the electrons and the Coulomb energy in the system, its anharmonicity (dependence of the frequency or zero-point energy on the lattice constant) can expand the equilibrium lattice constant by 1% or more for light atoms like Li and by much less for heavy atoms. Typically, the uncorrected lattice constant from DFT is compared to an experimental value corrected to the static-lattice case.

DFT in the formulation of Kohn and Sham gives the ground-state static-lattice energy as a functional of the electron density  $n(\mathbf{r})$  or its up- and down-spin components:

$$E = T_s[n_\uparrow, n_\downarrow] + \int d^3r n(\mathbf{r})v(\mathbf{r}) + U[n] + E_{xc}[n_\uparrow, n_\downarrow] + V_{nn} . \quad (3-1)$$

The five terms on the right of Equation (3-1) represent the non-interacting kinetic energy of the electrons, the Coulomb interaction between electrons and nuclei, the Hartree energy of electron-electron repulsion, the exchange-correlation energy of the electrons, and the nucleus-nucleus repulsion, respectively. The first three terms can be

calculated exactly from energy-minimizing occupied orbitals for a given set of nuclear positions, the exchange- correlation energy can only be approximated in practice.

Semi-local approximations to the exchange-correlation energy are widely used for solids, because they are often nonempirical and are computationally faster than all other methods. Because of the slowly varying density in many *sp*-bonded solids near equilibrium, the semi-local functionals can work well [77], although they can make larger errors for other solids in which there are important long-range van der Waals interactions or in which electrons are shared over stretched bonds [77]. We will test five nonempirical local and semi-local functionals belonging to different levels of a ladder of approximations: the local density approximation (LDA) [10, 22], Perdew-Burke-Ernzerhof (PBE) [78] and Perdew-Burke-Ernzerhof for solids (PBEsol) [41] that belong to the generalized gradient approximation (GGA) level [31, 33, 78], and Tao-Perdew-Staroverov-Scuseria (TPSS) [79] and revised Tao-Perdew-Staroverov-Scuseria (revTPSS) [48] that belong to the meta-GGA level. The early and simple local spin density approximation (LSDA) gives lattice constants that are too short for solids and overestimated atomization energies. The PBE GGA predicts reasonable but too-long lattice constants and improves atomization energies. The TPSS meta-GGA predicts lattice constants only a little smaller than those of PBE but gives better atomization energies for molecules than PBE does. While PBE is a general-purpose GGA for atoms, molecules, and solids, the PBEsol [41, 80, 81] GGA has a diminished gradient dependence [82] designed specifically for solids and solid surfaces near equilibrium. The revTPSS meta-GGA, which takes insights from the PBEsol construction, gives lattice

constants as accurate as those of PBEsol while keeping the atomization energies as accurate as those of TPSS.

### **3.2 The ZPAE Correction: From a Simple Model to a Phonon Model**

The widely used zero-point anharmonic expansion (ZPAE) method gives the lattice constant correction to a DFT calculation at zero temperature. A simple model for the contribution of zero-point anharmonic expansion (ZPAE) to the lattice constant of a solid was proposed in Ref. [83] and used in Refs. [84-88] to test various density functionals. Ref. [86] introduced the large test set of 58 solids, which we use here. The more accurate but more computationally demanding phonon model for zero-point anharmonic contribution has been used, e.g., in Refs. [89] and [90]. Ref. [90] compared the simple and phonon models for a test set about half the size of ours, including some solids in diamond and zinc-blende structures, and reached conclusions similar to but less analyzed than those we reach here. In particular, we will show that the simple model is reasonably accurate except in diamond and zinc-blende structures, where its error arises mainly from the Dugdale-MacDonald model for the Grüneisen parameter and less from the Debye model for vibrational energy. Our work was well under way before we learned of Ref. [90].

In the simple model, the zero-point energy is given by the Debye model [18], and the volume expansion of it is given by the Dugdale-MacDonald model [91]. The inputs of the simple model are the Debye temperature, the bulk modulus, and the first derivative of

the bulk modulus with pressure. The first two quantities can be found from accurate experimental values [86] for the low-temperature specific heat and compressibility. For the first derivative of the bulk modulus, which is not given so accurately by experiment, we use theoretical TPSS values, as was done in Ref. [84].

The derivation of the simple model is given with telegraphic brevity in Appendix A of Ref. [83]. Here we show how to derive the simple model correction, starting from Eq. (A1) of that appendix, where all quantities are “per atom”. We begin with the total energy per atom

$$\varepsilon(v) = \varepsilon^0(v) + \frac{3}{2}\hbar\omega(v), \quad (3-2)$$

where  $v$  is the volume per atom, which for the solids we consider is equal to  $a^3/2$  for the body-centered cubic (bcc) and CsCl structures,  $a^3/4$  for the face-centered cubic (fcc) structure, and  $a^3/8$  for the rocksalt, diamond, and zinc-blende structures. Here  $a$  is the cube-side lattice constant,  $\varepsilon^0(v)$  is the ground-state energy given by a DFT calculation without the zero-point energy correction, and  $\frac{3}{2}\omega$  is the phonon zero-point energy per atom, where  $\omega$  is an average phonon frequency.

The Taylor expansion to second order of  $\varepsilon(v)$  around  $v_0$  is

$$\varepsilon(v) = \varepsilon^0(v_0) + \frac{\alpha}{2}(v - v_0)^2 + \frac{3}{2}\hbar\omega(v_0) + \beta(v - v_0), \quad (3-3)$$

where  $v_0$  is the equilibrium volume calculated from the DFT method. In Equation (3-3), the first two terms on the right arise from the DFT calculation, and the second two terms arise from the zero-point vibrational energy. Here,

$$\alpha = \left. \frac{d^2 \varepsilon^0}{dv^2} \right|_{v_0} = \frac{B_0}{v_0}, \quad (3-4)$$

where  $B_0$  is the equilibrium bulk modulus. For the zero-point energy, the average frequency  $\omega$  is nearly linear in volume around the equilibrium volume, and

$$\beta = \frac{3}{2} \left. \frac{d\omega}{dv} \right|_{v_0}. \quad (3-5)$$

Since the Grüneisen parameter at equilibrium is

$$\gamma_0(v) = - \left. \frac{v}{\omega} \frac{d\omega}{dv} \right|_{v_0}, \quad (3-6)$$

we find

$$\beta = - \frac{3}{2} \gamma_0 \frac{\omega_0}{v_0}. \quad (3-7)$$

Because the derivative of  $\varepsilon$  with respect to  $v$  is equal to zero at the real equilibrium position, from Equation (3-3) we have

$$\alpha(v - v_0) + \beta = 0. \quad (3-8)$$

So the correction to the DFT-calculated volume is

$$\Delta v = (v - v_0) = - \frac{\beta}{\alpha} = \frac{3}{2} \gamma_0 \frac{\omega_0}{B_0}. \quad (3-9)$$

So far, the volume correction is derived without serious approximation. When we choose the Grüneisen parameter as

$$\gamma_0(v) \approx \frac{1}{2} (B_1 - 1) \quad (3-10)$$



from the Dugdale-MacDonald model [91] (where  $B_1$  is the pressure derivative of the bulk modulus at equilibrium) and combine it with the Debye approximation

$$\omega = \frac{3}{4} k_B \theta_D , \quad (3-11)$$

where  $\theta_D$  is the Debye temperature, we get the simple model

$$\frac{\Delta v}{v_0} = \frac{3\Delta a}{a_0} = \frac{9}{16} (B_1 - 1) \frac{k_B \theta_D}{B_0 v_0}. \quad (3-12)$$

The underlying picture of the Debye and Dugdale-MacDonald approximations is a crystal with one atom per primitive cell. The approximations may work, but less reliably, when there is more than one atom per cell. The Dugdale-MacDonald model has a correct limit: The anharmonic effects vanish for a harmonic crystal ( $B_1 = 1$ ).

To see how well the simple model works, we compare the simple model to our phonon model. In the phonon model, the zero-point energy is calculated from the average frequency of lattice vibration using Quantum Espresso (QE) code instead of the Debye model. It is

$$\varepsilon_{vib} = \frac{\int_0^{\frac{3}{2}} g(\omega) d\omega}{\int_0^{\frac{3}{2}} g(\omega) d\omega} \quad (3-13)$$

where  $g(\omega)$  is the density of phonon states.  $\int_0^{\frac{3}{2}} g(\omega) d\omega$  is the number of modes of vibration per primitive cell. For a monatomic crystal  $\int_0^{\frac{3}{2}} g(\omega) d\omega = 3$ : for a diatomic structure,  $\int_0^{\frac{3}{2}} g(\omega) d\omega = 6$ .

Also, we can calculate the Grüneisen parameter at equilibrium  $\gamma_0(v)$  from its definition using the curve of zero-point energy versus lattice constant.

$$\gamma_0(v) = -\frac{1}{3} \frac{a_0}{\varepsilon_{vib0}} \frac{d\varepsilon_{vib}}{da} \quad (3-14)$$

where  $a_0$  is the equilibrium lattice constant calculated from the DFT method and  $\varepsilon_{vib0}$  is the zero-point energy at  $a_0$ .  $\frac{d\varepsilon_{vib}}{da}$  can be evaluated around the equilibrium lattice constant.

### 3.3 Results and Discussions

#### 3.3.1 Comparison of the Two ZPAE Corrections

A set of 58 cubic solids [86] was considered (Table 1). The phonon zero-point energy was calculated as a function of the lattice constant. The computations were realized using QE code [71]. The PBE functional was used in our phonon calculation, with PBE pseudopotentials [92]. QE code uses density functional perturbation theory (DFPT) [11] to calculate the interatomic force constants from first principles, which leads to the phonon frequencies. The first Brillouin zone was sampled with the  $12 \times 12 \times 12$   $k$ -mesh for most solids. In addition,  $6 \times 6 \times 6$   $q$ -points were used for calculating the dynamic matrix, which gives the phonon frequencies at a specified  $q$  point in the Brillouin zone. Then the density of phonon states is calculated from a  $15 \times 15 \times 15$  mesh, which is interpolated from the  $6 \times 6 \times 6$   $q$ -points.

The QE code uses a plane-wave basis with pseudopotentials. For the elements Rb and Hf, the pseudopotentials are not provided on the QE web site, so we do not calculate the

phonon zero-point energy of Rb, HfC and HfN, which are in our set of solids. For solid VN and NbN, the rocksalt phase is not stable at zero temperature [93], and for them we found nonpositive phonon frequencies in our calculation, which confirms that instability. So we do not report phonon values for VN and NbN either.

In Table 1 we present the zero-point energy, Grüneisen parameter, and lattice constant correction using the simple model and the phonon model. Experimental Debye temperature, lattice constants, and bulk moduli were used (from Ref. [86]), which we list in our supplementary material [75]. The pressure derivative of the bulk modulus was calculated from the TPSS functional.

**Table 1** The zero-point energy per atom (columns 1 and 2), the Grüneisen parameter (columns 3 and 4), and the lattice constant correction as a percentage of the experimental lattice constant using the simple model and phonon correction (columns 5 and 6, respectively).

Solid <sup>a,b</sup>	$3/2 \ \omega_D$ <sup>c</sup>	$3/2 \ \omega_0$ <sup>d</sup>	$\gamma_{DM}$ <sup>e</sup>	$\gamma_0$ <sup>f</sup>	$\frac{\Delta a_{SM}}{a_{expt.}}(\%)$	$\frac{\Delta a_{phonon}}{a_{expt.}}(\%)$
Li(A2) (1,2)	0.0333	0.0406	1.2755	0.9434	0.831	0.748
Na(A2) (1,2)	0.0153	0.0146	1.3223	1.5435	0.382	0.425
K(A2) (1,2)	0.0088	0.0090	1.1779	1.4180	0.210	0.259
Rb(A2) (1,2)	0.0054		0.7946		0.085	
Ca(A1) (1,4)	0.0223	0.0209	1.0250	1.2406	0.154	0.175
Sr(A1) (1,4)	0.0143	0.0103	1.2114	1.2543	0.135	0.101
Ba(A2) (1,2)	0.0107	0.0095	0.7823	0.6839	0.076	0.059
V(A2) (1,2)	0.0368	0.0325	1.3295	1.7719	0.116	0.137
Nb(A2) (1,2)	0.0267	0.0272	1.3480	1.7514	0.063	0.084
Ta(A2) (1,2)	0.0233	0.0217	2.0261	2.1602	0.072	0.072
Mo(A2) (1,2)	0.0436	0.0391	1.6008	1.8187	0.088	0.090
W(A2) (1,2)	0.0388	0.0376	1.2070	1.0957	0.050	0.044
Fe(A2) (1,2)	0.0456	0.0450	2.1346	1.8522	0.264	0.226
Rh(A1) (1,4)	0.0465	0.0367	2.1495	2.4203	0.145	0.129
Ir(A1) (1,4)	0.0407	0.0302	2.0015	2.3073	0.087	0.074

Ni(A1) (1,4)	0.0436	0.0436	1.9287	1.6726	0.220	0.191
Pd(A1) (1,4)	0.0266	0.0293	2.3443	2.4352	0.117	0.134
Pt(A1) (1,4)	0.0233	0.0251	2.1693	2.5823	0.065	0.083
Cu(A1) (1,4)	0.0333	0.0353	2.0179	1.9153	0.216	0.218
Ag(A1) (1,4)	0.0218	0.0237	2.4210	2.2937	0.154	0.158
Au(A1) (1,4)	0.0160	0.0195	2.4176	2.5853	0.068	0.089
Al(A1) (1,4)	0.0415	0.0411	1.7924	1.8695	0.305	0.316
C(A4) (2,8)	0.2162	0.1894	1.3584	0.8113	0.624	0.327
Si(A4) (2,8)	0.0625	0.0610	1.6134	0.9063	0.271	0.149
Ge(A4) (2,8)	0.0363	0.0338	1.9000	1.2914	0.215	0.136
Sn(A4) (2,8)	0.0194	0.0215	2.0703	1.4068	0.119	0.089
Pb(A1) (1,4)	0.0102	0.0099	2.0798	2.4276	0.078	0.088
LiF(B1) (2,8)	0.0710	0.0681	1.6392	1.3975	1.104	0.903
LiCl(B1) (2,8)	0.0409	0.0339	1.8958	2.1750	0.703	0.668
NaF(B1) (2,8)	0.0477	0.0526	1.7637	1.8814	0.714	0.840
NaCl(B1) (2,8)	0.0311	0.0298	1.8997	1.9916	0.542	0.545
MgO(B1) (2,8)	0.0917	0.0762	1.5496	1.6760	0.494	0.444
MgS(B1) (2,8)	0.0630	0.0399	1.3654	1.7913	0.326	0.271
CaO(B1) (2,8)	0.0628	0.0894	1.7341	1.5286	0.365	0.458
TiC(B1) (2,8)	0.0911	0.0840	1.6262	1.4557	0.335	0.276
TiN(B1) (2,8)	0.0734	0.0823	1.6270	1.8301	0.242	0.305
ZrC(B1) (2,8)	0.0679	0.0691	1.4781	1.4324	0.200	0.197
ZrN(B1) (2,8)	0.0679	0.0622	1.6413	1.7809	0.206	0.205
HfC(B1) (2,8)	0.0536		1.5300		0.145	
HfN(B1) (2,8)	0.0590		1.3706		0.159	
VC(B1) (2,8)	0.0590	0.0783	1.5643	1.9402	0.181	0.297
VN(B1) (2,8)	0.0732		1.6391		0.269	
NbC(B1) (2,8)	0.0738	0.0714	1.6240	1.7236	0.191	0.196
NbN(B1) (2,8)	0.0708		1.6364		0.203	
FeAl(B2) (2,2)	0.0498	0.0520	1.5321	1.6112	0.248	0.273
CoAl(B2) (2,2)	0.0485	0.0539	1.5767	1.5645	0.215	0.237
NiAl(B2) (2,2)	0.0390	0.0455	1.6301	1.8242	0.170	0.222
BN(B3) (2,8)	0.1648	0.1718	1.3297	0.8454	0.536	0.355
BP(B3) (2,8)	0.0955	0.1003	1.4024	0.8298	0.403	0.250
BAs(B3) (2,8)	0.0776	0.0818	1.5245	1.1868	0.336	0.276
AlP(B3) (2,8)	0.0570	0.0538	1.4979	0.9866	0.301	0.187
AlAs(B3) (2,8)	0.0283	0.0435	1.6012	1.1949	0.144	0.166
GaN(B3) (2,8)	0.0582	0.0778	1.7133	0.9759	0.235	0.179
GaP(B3) (2,8)	0.0431	0.0344	1.8919	1.1896	0.247	0.124
GaAs(B3) (2,8)	0.0333	0.0322	1.7991	1.1947	0.188	0.121

InP(B3) (2,8)	0.0311	0.0377	1.8653	1.2787	0.173	0.144
InAs(B3) (2,8)	0.0239	0.0266	1.9688	1.1212	0.156	0.099
SiC(B3) (2,8)	0.1194	0.1084	1.4656	0.9086	0.402	0.226

<sup>a</sup> The Strukturbericht symbols (in parentheses) are used for the structures as follows: A1, fcc; A2, bcc; A4, diamond; B1, rocksalt; B2, CsCl; B3, zinc blende.

<sup>b</sup> The two numbers in parentheses are the number of atoms per primitive cell followed by the number of atoms per conventional cubic cell.

<sup>c</sup> From the simple model. The unit is electron volts.

<sup>d</sup> From the phonon model. The unit is electron volts.

<sup>e</sup> From the Dugdale-MacDonald model.

<sup>f</sup> From the curve of phonon zero-point energy versus lattice constant.

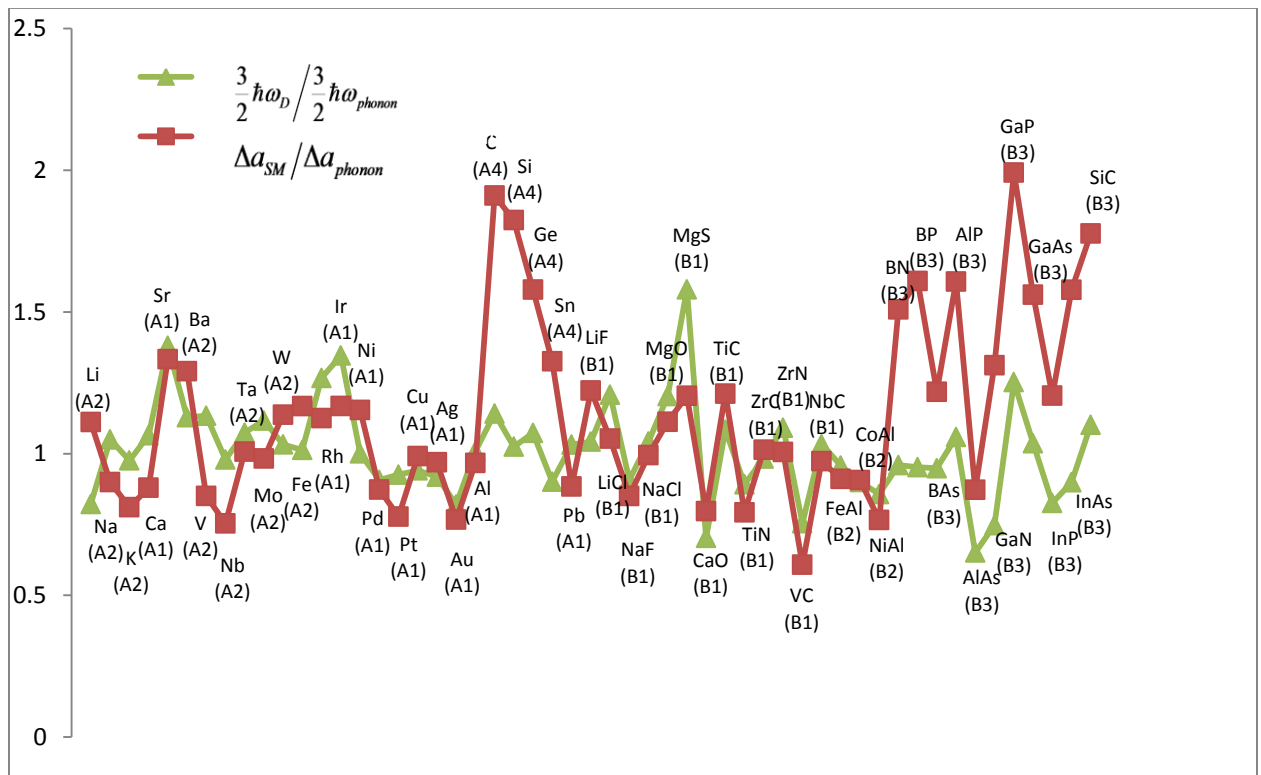


Fig. 3 (Color online) The light gray (green) line is the ratio of the zero-point energy approximated by the Debye model to that computed from the phonon average frequency. The dark gray (red) line is the ratio of the lattice constant correction ( $\Delta a$ ) alculated by the simple model to that calculated by the phonon model.

In Fig. 3 and Fig. 4, we show the ratio of the zero-point energy, the ratio of the Grüneisen parameter, and the ratio of lattice constant correction found from the simple model to that found from the phonon model. From Fig. 3 we see that the zero-point

energy approximated by the Debye model is reasonably accurate. For the monatomic crystal (one atom per primitive cell: A1 and A2), the ratio of the zero-point energy is on average bigger than 1. Except for Na and Au which have ratios smaller than 0.9, the ratios for the other monatomic solids are all above 0.9. This is because the Debye model uses a linear approximation for the dispersion curve. However, the real dispersion curve at large wavevector in a monatomic solid has smaller frequencies than those of the Debye model, which means that the zero-point energy is overestimated by the Debye model. For a diatomic crystal (two atoms per primitive cell: A4 and B1-B3), the ratio of the zero-point energy is smaller than 1 on average. Except for LiF, MgO, MgS, and GaP, which have ratios larger than 1.2, the ratios are all under 1.2 and many are under 1.0. For a crystal with two atoms per unit cell, the Debye model continues to use a linear (in the extended zone scheme) extrapolation of the small-wavevector average acoustic dispersion, even for the optical modes. But the optical modes might be better approximated by an Einstein model, in which frequency is independent of wavevector. Thus, the Debye model tends to underestimate the optical phonon zero-point energy when the actual frequency gap between optical and acoustic modes is large and to overestimate it when this gap is small (as it is for LiF, MgO, MgS, and GaP).

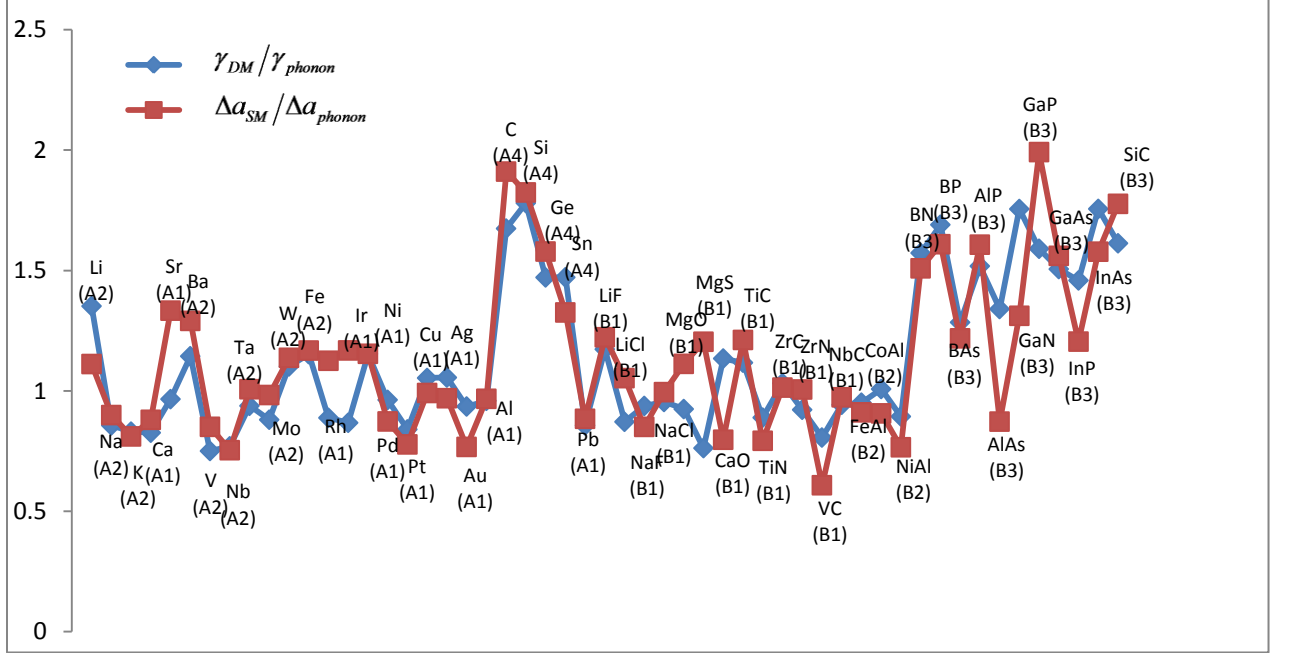


Fig. 4 (Color online) The light gray (blue) line is the ratio of the Grüneisen parameter approximated by the Dugdale-MacDonald model to that approximated by the phonon model. The dark gray (red) line is the ratio of the lattice constant correction ( $\Delta a$ ) calculated by the simple model to that calculated by the phonon model. Note the similarity of the two curves, which shows that most of the error of the simple model arises from the Dugdale-MacDonald approximation.

In Fig. 4, the Grüneisen parameter ratio also fluctuates around and close to 1, except in the A4 and B3 structures. For the solids of A4 and B3 structures, the Grüneisen parameter given by the Dugdale-MacDonald model is at least  $\sim 50\%$  bigger than that given by the phonon model-and sometimes more. Because of that, the lattice constant correction given by the simple model is overestimated for solids of the A4 and B3 structures. It appears that covalent-bonding non-close-packed structures do not follow the Dugdale-MacDonald model.

### 3.3.2 Performance of Semi-Local Functionals for Lattice Constants

We modified the current version of BAND [72-74], which implements revTPSS only non-self-consistently, to implement it self-consistently. For revTPSS, the exchange-correlation energy involves the kinetic energy density  $\tau(\mathbf{r})$ , which is not an explicit functional of the density  $n(\mathbf{r})$ . So the exchange-correlation potential,  $v_{xc}(\mathbf{r}) = \delta E_{xc} / \delta n(\mathbf{r})$ , is not calculated directly. The partial integration method [94] is used for calculating the matrix elements of the exchange-correlation potential. All orbitals are treated numerically in BAND. We derived the partial derivatives for the revTPSS functional and tested their correctness by numerically differentiating the energy density with respect to those independent variables, including spin densities, gradients and kinetic energy density. Relativistic effects are included in the zero-order regular approximation.

Lattice constants and bond lengths can be computed two ways: by minimizing the total energy and by zeroing out the Hellmann-Feynman forces and stresses. The results of the second approach are more sensitive to the orbitals than those of the first. The results are expected to agree only at self-consistency, so the agreement shown in Table 2 is a good test of self-consistency.



**Table 2** Test of revTPSS self-consistency employing the bond lengths (in angstroms) of the Li, N, and Ca dimers.

Molecule	Energy <sup>a</sup>	Grad=0 <sup>b</sup>	Difference
<i>Li</i> <sub>2</sub>	2.75687	2.75671	-0.00016
<i>N</i> <sub>2</sub>	1.10069	1.10069	-0.00005
<i>Ca</i> <sub>2</sub>	4.10702	4.10675	-0.00026

<sup>a</sup>“Energy” means calculating a revTPSS total energy for bond lengths separated by 0.01 bohr, fitting the result, and minimizing the fitted energy.

<sup>b</sup>“Grad = 0” means optimizing the geometry until the forces are less than  $10^{-8}$  hartree per bohr.

The BAND program uses a mixed Slater-type and numerical-type orbital basis set. In our lattice constant calculation, the quadruple zeta plus quadrupole polarization basis set is used, which is the biggest basis set in BAND code. The largest number of  $k$ -points (parameter 7) is used for solving the Kohn-Sham equations. There are 84  $k$ -points for bcc and 196  $k$ -points for fcc in the irreducible wedge. The lattice constants are calculated by fitting the energy curve using the stabilized jellium equation of state (SJEOS) [83]. The functionals LSDA, PBE, PBEsol and TPSS are evaluated with revTPSS orbitals.

In Table 3, the experimental lattice constants are corrected for ZPAE. Phonon model correction is used when available. For the solids Rb, HfC, HfN, VN and NbN, as discussed earlier, the simple model is used. The theoretical lattice constants calculated by various functionals are compared to the experimental lattice constants corrected to the static-lattice case. The mean error (ME), the mean absolute error (MAE), the mean relative error (MRE, in percent), and the mean absolute relative error (MARE, in percent) are given for each functional.

**Table 3** Theoretical lattice constants (in angstroms) calculated from BAND code using LSDA, PBE, PBEsol, TPSS, and revTPSS functionals. The revTPSS density is used for all calculations. The experimental lattice constants are corrected for ZPAE.

Solid	LSDA BAND	PBE BAND	PBEsol BAND	TPSS BAND	revTPSS BAND	Expt.- $\Delta a$
Li	3.368	3.429	3.429	3.446	3.434	3.451
Na	4.051	4.197	4.174	4.249	4.222	4.207
K	5.050	5.281	5.220	5.369	5.325	5.211
Rb <sup>a</sup>	5.374	5.665	5.571	5.768	5.716	5.580
Ca	5.321	5.521	5.449	5.540	5.520	5.555
Sr	5.779	6.013	5.911	6.023	6.001	6.042
Ba	4.732	5.022	4.874	5.002	4.978	5.004
V	2.924	2.997	2.958	2.975	2.968	3.024
Nb	3.246	3.310	3.272	3.294	3.284	3.293
Ta	3.298	3.347	3.320	3.329	3.317	3.299
Mo	3.110	3.161	3.130	3.147	3.137	3.141
W	3.122	3.170	3.141	3.153	3.139	3.161
Fe	2.749	2.834	2.788	2.804	2.793	2.855
Rh	3.749	3.827	3.777	3.800	3.780	3.793
Ir	3.812	3.872	3.832	3.851	3.829	3.832
Ni	3.419	3.517	3.461	3.475	3.455	3.509
Pd	3.832	3.932	3.869	3.887	3.862	3.876
Pt	3.895	3.971	3.920	3.943	3.916	3.913
Cu	3.518	3.630	3.565	3.577	3.551	3.595
Ag	4.001	4.150	4.055	4.086	4.051	4.063
Au	4.039	4.147	4.074	4.103	4.069	4.061
Al	3.982	4.037	4.014	4.011	4.008	4.019
C	3.532	3.571	3.553	3.569	3.559	3.555
Si	5.402	5.468	5.432	5.452	5.438	5.422
Ge	5.624	5.764	5.679	5.723	5.680	5.644
Sn	6.475	6.659	6.543	6.612	6.560	6.476
Pb	4.882	5.040	4.935	4.981	4.939	4.912
LiF	3.915	4.064	4.005	4.031	4.013	3.974
LiCl	4.972	5.147	5.063	5.093	5.085	5.072
NaF	4.502	4.700	4.630	4.706	4.675	4.570
NaCl	5.466	5.695	5.606	5.705	5.671	5.565
MgO	4.162	4.255	4.216	4.237	4.233	4.188
MgS	5.127	5.228	5.184	5.228	5.222	5.188

CaO	4.709	4.832	4.769	4.809	4.808	4.781
TiC	4.260	4.332	4.293	4.328	4.316	4.318
TiN	4.171	4.247	4.204	4.239	4.231	4.226
ZrC	4.639	4.708	4.668	4.707	4.694	4.687
ZrN	4.524	4.594	4.552	4.588	4.580	4.576
HfC <sup>a</sup>	4.571	4.655	4.609	4.646	4.624	4.631
HfN <sup>a</sup>	4.470	4.553	4.506	4.540	4.524	4.513
VC	4.087	4.154	4.116	4.146	4.132	4.148
VN <sup>a</sup>	4.041	4.116	4.073	4.108	4.097	4.130
NbC	4.425	4.484	4.449	4.481	4.465	4.461
NbN <sup>a</sup>	4.355	4.422	4.381	4.417	4.404	4.383
FeAl	2.811	2.868	2.840	2.850	2.842	2.881
CoAl	2.793	2.851	2.823	2.832	2.822	2.854
NiAl	2.832	2.892	2.862	2.872	2.862	2.881
BN	3.581	3.624	3.605	3.621	3.615	3.594
BP	4.491	4.548	4.520	4.544	4.529	4.527
BAs	4.733	4.809	4.768	4.799	4.774	4.764
AlP	5.433	5.504	5.468	5.492	5.482	5.450
AlAs	5.631	5.728	5.676	5.702	5.682	5.649
GaN	4.457	4.549	4.499	4.532	4.518	4.523
GaP	5.392	5.506	5.439	5.488	5.460	5.441
GaAs	5.607	5.751	5.664	5.716	5.675	5.641
InP	5.829	5.963	5.882	5.949	5.918	5.858
InAs	6.026	6.188	6.089	6.157	6.113	6.048
SiC	4.329	4.378	4.356	4.366	4.357	4.348
ME <sup>b</sup>	<b>-0.064</b>	<b>0.043</b>	<b>-0.010</b>	<b>0.030</b>	<b>0.010</b>	
MAE <sup>b</sup>	<b>0.064</b>	<b>0.049</b>	<b>0.028</b>	<b>0.040</b>	<b>0.030</b>	
MRE (%) <sup>b</sup>	<b>-1.478</b>	<b>0.894</b>	<b>-0.295</b>	<b>0.549</b>	<b>0.115</b>	
MARE (%) <sup>b</sup>	<b>1.478</b>	<b>1.048</b>	<b>0.641</b>	<b>0.856</b>	<b>0.675</b>	

<sup>a</sup>For the solids Rb, HfC, HfN, VN, and NbN, the simple model is used; for all other solids, phonon correction is used.

<sup>b</sup>Error statistics are in boldface.

From Table 3, we can clearly see that the ME, MAE, MRE and MARE are all reduced from LDA to PBE GGA and then further reduced to the higher-level TPSS meta-GGA and revTPSS meta-GGA. PBEsol gives lattice constants as good as revTPSS. TPSS and PBE have similar statistical errors, although TPSS is slightly better than PBE. LDA underestimates the lattice constants for nearly all solids, as expected.

Table 4 shows the relative errors of the lattice constants, which are always negative for LSDA but not for the other functionals. When the relative errors of revTPSS are ordered from most positive to most negative, as in Table 4, several trends emerge: (1) The most positive errors tend to occur for ionic solids with large polarizable negative ions and for heavy alkali metals with large ionic cores, where the long-range van der Waals attraction missing in revTPSS should reduce the error [95][95]. (2) The most negative errors occur for the 3d transition metals, where very localized but overlapped 3d orbitals produce a density very different from the atomic and slowly varying paradigms of the meta-GGA form. The 3d metals may require a non-van-der-Waals kind of full nonlocality also missing in revTPSS. Indeed the relative error becomes less negative from 3d to 4d to 5d as the d orbitals become more diffuse.

**Table 4** Relative errors (in percent) in lattice constants with respect to the ZPAE-corrected experimental values, ordered from the most positive value to the least positive value of revTPSS.

	Type of solid	LSDA	PBE	PBEsol	TPSS	revTPSS
Rb	SM	-3.70	1.52	-0.16	3.37	2.44
NaF	II	-1.50	2.84	1.31	2.98	2.29
K	SM	-3.09	1.34	0.17	3.02	2.17
NaCl	II	-1.76	2.35	0.74	2.52	1.92
Sn	SC	-0.01	2.83	1.03	2.09	1.29
InAs	SC	-0.37	2.32	0.67	1.80	1.08
MgO	II	-0.63	1.58	0.66	1.17	1.06
InP	SC	-0.48	1.80	0.42	1.57	1.04
LiF	II	-1.47	2.26	0.79	1.45	0.98
MgS	II	-1.18	0.78	-0.08	0.76	0.65
Ge	SC	-0.36	2.12	0.61	1.40	0.63
GaAs	SC	-0.61	1.95	0.41	1.33	0.59
AlP	SC	-0.31	1.00	0.34	0.77	0.59
BN	SC	-0.37	0.82	0.31	0.76	0.59

AlAs	SC	-0.31	1.40	0.48	0.95	0.58
Ta	TM	-0.03	1.48	0.65	0.91	0.57
CaO	II	-1.52	1.06	-0.25	0.59	0.56
Pb	SM	-0.60	2.61	0.47	1.41	0.56
NbN	II	-0.64	0.88	-0.06	0.77	0.49
Na	SM	-3.72	-0.25	-0.78	0.99	0.36
GaP	SC	-0.91	1.20	-0.04	0.85	0.35
Si	SC	-0.37	0.85	0.19	0.56	0.29
LiCl	II	-1.97	1.48	-0.18	0.42	0.25
HfN	II	-0.95	0.90	-0.15	0.60	0.24
BAs	SC	-0.64	0.96	0.09	0.73	0.22
SiC	SC	-0.44	0.69	0.18	0.41	0.21
Au	TM	-0.56	2.10	0.32	1.03	0.20
ZrC	II	-1.01	0.46	-0.40	0.44	0.16
TiN	II	-1.30	0.49	-0.52	0.29	0.11
C	SC	-0.66	0.44	-0.06	0.37	0.10
NbC	II	-0.81	0.50	-0.28	0.44	0.10
ZrN	II	-1.13	0.41	-0.51	0.28	0.09
Pt	TM	-0.45	1.50	0.18	0.78	0.09
BP	SC	-0.78	0.46	-0.15	0.39	0.05
TiC	II	-1.34	0.32	-0.59	0.23	-0.04
Ir	TM	-0.53	1.04	-0.01	0.49	-0.09
GaN	SC	-1.45	0.57	-0.53	0.21	-0.12
Mo	TM	-0.98	0.63	-0.37	0.20	-0.15
HfC	II	-1.30	0.51	-0.48	0.32	-0.15
Al	SM	-0.94	0.45	-0.14	-0.21	-0.27
Nb	TM	-1.44	0.52	-0.65	0.03	-0.29
Ag	TM	-1.52	2.15	-0.18	0.57	-0.29
Rh	TM	-1.15	0.91	-0.42	0.19	-0.35
Pd	TM	-1.14	1.45	-0.17	0.29	-0.36
VC	II	-1.47	0.15	-0.77	-0.03	-0.39
Li	SM	-2.42	-0.63	-0.62	-0.15	-0.49
Ba	SM	-5.45	0.36	-2.61	-0.05	-0.52
Ca	SM	-4.21	-0.61	-1.92	-0.28	-0.63
NiAl	AM	-1.69	0.40	-0.63	-0.30	-0.65
W	TM	-1.23	0.31	-0.63	-0.25	-0.67
Sr	SM	-4.36	-0.47	-2.17	-0.32	-0.68
VN	II	-2.15	-0.33	-1.38	-0.54	-0.81
CoAl	AM	-2.14	-0.11	-1.11	-0.79	-1.12
Cu	TM	-2.16	0.98	-0.85	-0.51	-1.23

FeAl	AM	-2.43	-0.45	-1.42	-1.07	-1.37
Ni	TM	-2.57	0.21	-1.37	-0.99	-1.55
V	TM	-3.30	-0.89	-2.17	-1.63	-1.86
Fe	TM	-3.70	-0.72	-2.35	-1.78	-2.15

SM, simple metal; TM, transition metal; II, ionic insulator; SC, semiconductor (A4 or B3 structures); AM, alloy metal.

In Table 5, we show the ZPAE effect on the revTPSS lattice constants. The revTPSS lattice constants are compared with the corrected experimental lattice constant. For the phonon model correction, all statistical errors (ME, MAE, MRE and MARE) are smaller than for the simple model correction.

**Table 5** Error statistics for the revTPSS lattice constant, compared with corrected experimental lattice constant using two different corrections, for the solids listed in Table 3, excepting Rb, HfC, HfN, VN and NbN for the phonon model.

	Simple model	Phonon model
ME	0.011	0.009
MAE	0.031	0.029
MRE (%)	0.133	0.084
MARE (%)	0.705	0.661

To check the performance of these functionals in a dispersion-dominated interaction system, we show the lattice constants of graphite in Table 6. The in-plane lattice constant is fixed at the experimental value 2.464 Å and a search is made for the equilibrium interlayer distance  $c/2$ , where  $c$  is the lattice constant. Due to its tendency of underestimate lattice constants, which compensates for the absence of long-range dispersion in graphite, LDA spuriously predicts the most precise lattice constant. As expected, PBE yields a lattice constant that is too large, whereas PBEsol puts the lattice constant between that of LDA and that of PBE. TPSS barely binds graphite, with the minimum at 10.0 Å on VASP code, which is  $\sim 5$  Å smaller than that given in Ref. [86],

and 8.8 Å on BAND code. This is probably because the TPSS calculations of Ref. [86] were non-self-consistent and the binding curve of TPSS is very flat. revTPSS performs similarly to TPSS, showing that both are unable to capture the long-range part of the dispersion or van der Waals interaction.

**Table 6** The inter-layer equilibrium lattice constant (in angstroms) of graphite, calculated from BAND and VASP.

Functionals	LDA	PBE	PBEsol	TPSS	revTPSS	expt.
c (BAND)	6.7	8.7	7.4	8.8	8.8	6.71
c (VASP)	6.7	8.8	7.4	10.0	10.1	6.71

### 3.3.3 Self-Consistency Effect on the Lattice Constant Calculation

Refs. [85-87] employed a non-self-consistent implementation of the meta-GGAs. Ref. [96] implemented the revTPSS meta-GGA self-consistently in Vienna ab initio simulation package (VASP) code, and Ref. [88] applied revTPSS to a carbon monoxide molecule on transition-metal surfaces. In our calculation, we implement revTPSS self-consistently in the solid state band-structure code BAND.

Self-consistent meta-GGA is much more time consuming than self-consistent LDA, especially for an all-electron calculation as in the BAND code. Sometimes, a non-self-consistent calculation is effective and computationally necessary. We define the self-consistency effect on the lattice constant in the following way: For a given energy functional, minimize energy versus lattice constant using the self-consistent density for that functional and then the density for another functional, e.g., LDA, and see how much the lattice constant differs. The self-consistency effect for the PBE GGA is very small, on the order of 0.001-0.002 Å, even for soft solids like Ca, Sr, Ba, and Rb. So we expect the self-consistency effect also to be small for the revTPSS meta-GGA. For most of our

solids, we can confirm this expectation, but we cannot do so for the soft solids. The self-consistency effects for the soft solids are shown in Table 7. We doubt whether these effects are real and suspect that they are simply a consequence of numerical error of revTPSS in BAND. We have not found such large revTPSS self-consistency effects with VASP. Perhaps they are only a reflection of the additional numerical errors that can arise in an all-electron code like BAND when the curve of total energy versus lattice constant is very flat. In any case, self-consistency is still important for the determination of bond lengths, bond angles, and lattice constants via Hellmann-Feynman forces and stresses, etc.

**Table 7** Lattice constants calculated (in angstroms) from the BAND and VASP code in revTPSS, self-consistently and from the LDA density. The difference between them is presented as a possible measure of the self-consistency effect, which is expected to be largest in soft solids like these with BAND, but not VASP.

functional	revTPSS	revTPSS	Difference	revTPSS	revTPSS	Difference
density	revTPSS	LDA	BAND	revTPSS	LDA	VASP
Ca	5.516	5.509	0.007	5.504	5.504	0.000
Rb	5.716	5.692	0.024	5.712	5.709	0.003
Sr	5.995	5.976	0.019	6.007	6.003	0.004
Ba	4.977	4.961	0.016	4.986	4.984	0.002

### 3.4 Conclusions

In this work, the revTPSS meta-GGA is implemented self-consistently in BAND code. The lattice constants of 58 solids are calculated using the density functionals LSDA, PBE, PBEsol, TPSS and revTPSS. LSDA makes the largest errors for solids, which makes its excellent performance for the bond lengths of diatomic molecules [51] all the



more surprising. The revTPSS meta-GGA predicts the lattice constant as well as the PBEsol GGA, and does so better than the other functionals tested. The largest positive or negative relative errors of the revTPSS lattice constants tend to occur in those solids in which some full nonlocality, absent in revTPSS, might be expected (section III). Overall, revTPSS appears to be the best of the semi-local functionals tested here, since it also produces generally the most accurate atomization energies of molecules [48], desorption energies of molecules from metal surfaces [88], and surface energies of metals [48, 88].

The experimental lattice constant is corrected for ZPAE in two ways. The simple model gives reasonable results for most solids. However, it overestimates the correction by about a factor of two for diamond and zinc-blende structures. This simple model is based on the Debye model for vibrational energy and the Dugdale-MacDonald model for the Grüneisen parameter. The underlying picture is thus that of a solid with one atom per primitive cell. The simple model can also work, but does so unreliably, for a solid with two atoms per unit cell; it fails for the covalent diamond and zinc-blende structures, where the Dugdale-MacDonald model is responsible for most of the failure. Diamond and zinc blende are open, covalent structures and are similar to each other. The phonon model in principle improves the zero-point energy and the Grüneisen parameter from those of the simple model. Compared to the simple model, the phonon model gives similar error statistics for lattice constants but requires more computational time, because the phonon calculation is expensive. However, the phonon model gives the more accurate zero-point energy correction, and we favor it as the benchmark ZPAE lattice constant correction. Moreover, the simple model requires a value for  $B_1$ , which is uncertain from experiment and even from calculation.

When phonon model corrections are unavailable, simple model corrections remain useful. However, greater accuracy can be achieved by empirically scaling the extreme right-hand side of Equation **(3-12)** by a factor of 0.66 for diamond and zinc-blende structures only. This factor zeros out the MRE of the simple model for the solids in our data set with these two structures.

Although thermal expansion due to phonon excitation is not our interest here, it can be addressed by the simple and phonon models.

## CHAPTER 4

# PERFORMANCE OF META-GGA FUNCTIONALS ON GENERAL MAIN GROUP THERMOCHEMISTRY, KINETICS, AND NONCOVALENT INTERACTIONS

This chapter was published as [97] “Performance of meta-gga functionals on general main group thermochemistry, kinetics, and noncovalent interactions”, P. Hao, J. Sun, B. Xiao, A. Ruzsinszky, G. I. Csonka, J. Tao, S. Glindmeyer, and J. P. Perdew, J. Chem. Theory Comput. DOI: 10.1021/ct300868x (2012).

### 4.1 Introduction

Kohn-Sham (KS) density functional theory (DFT) [10, 12] is one of the most widely used electronic structure theories for atoms, molecules and solids in areas of physics, chemistry and molecular biology. It simplifies a many-body wave-function problem to an auxiliary non-interacting one-electron problem, delivering in principle the

exact ground-state electron density and energy [10]. The performance of a KS-DFT calculation depends on the quality of the approximation to its exchange-correlation energy. Semi-local approximations [22, 30, 48, 79, 98] employ only local and semi-local information and so are efficient for large molecules or unit cells. They can be reasonably accurate for the near-equilibrium and compressed ground-state properties of “ordinary” matter, where neither strong correlation nor long-range van der Waals interaction is important. They can also serve as a base for the computationally more-expensive fully nonlocal approximations needed to describe strongly-correlated systems [77] and soft matter [99].

All semi-local functionals are computationally efficient. Among them, meta-generalized gradient approximations (meta-GGAs) are of special interest because they can achieve high simultaneous accuracy for atoms, molecules, solids, and surfaces at equilibrium. Meta-GGA [44, 48, 58, 79] is the highest rung at the semi-local level of Jacob’s ladder of DFT [52], which includes the kinetic energy density as an input in addition to the electron density and its density gradient. The local density approximation (LDA) [10, 22, 30, 98, 100] only depends on the electron density while the generalized gradient approximations (GGA) [34, 41, 98, 101-103] add the local electron density gradient. The inclusion of the kinetic energy density enables meta-GGAs to distinguish single-orbital regions from orbital overlap regions, allowing to predict accurate properties for molecules, surfaces, and solids [88]. This was highlighted in the study of the CO molecule adsorbed on transition-metal surfaces [88], where the revised Tao-Perdew-Staroverov-Scuseria (revTPSS) meta-GGA [48], unlike other tested LDA and GGAs,

predicts at the same time the accurate adsorption energy of the molecule to the surface and the lattice constant and surface energy of the metal substrate.

With the help of the kinetic energy density, the revTPSS [48] was constructed to recover the total energies of two paradigm densities - the uniform electron gas for condensed matter physics and the hydrogen atom for quantum chemistry. Moreover, revTPSS restores the second-order gradient expansion of a slowly-varying density for exchange over a wide range of densities as the PBEsol [41] GGA does, and thus improves the lattice constants of solids over its predecessor TPSS [79]. The regularized revTPSS (denoted as regTPSS) [104] was designed to remove the order-of-limits anomaly [104, 105] in the revTPSS exchange functional. The regTPSS gives atomization energies and lattice constants with an accuracy similar to that of revTPSS. The recently proposed meta-GGA made simple (MGGA\_MS) results from the study of the effect of the dependence of the meta-GGA [58] on kinetic energy density. The MGGA\_MS simplifies the construction of the exchange functional as an interpolation between the single-orbital regime (e.g., the hydrogen atom) and the slowly-varying density regime. For the correlation part of regTPSS and MGGA\_MS, a variant of the PBE correlation [58, 104] is used. In terms of atomization energies, surface energies, and lattice constants, the overall performance of MGGA\_MS is comparable to that of revTPSS. An interesting feature of MGGA\_MS for users is that it yields excellent binding energies for the W6 water clusters [106] - better than revTPSS, TPSS, and even PBE [58] - and thus clearly demonstrates its excellent performance for hydrogen bonds. In this study, we will further show that MGGA\_MS gives a quite good description for the noncovalent bonds with a systematic improvement over PBE, TPSS, revTPSS, and regTPSS.

Within the comfort zones, i.e., for “ordinary matter”, these newly developed meta-GGAs provide very accurate ground-state properties for molecules, surfaces, and solids [48, 58, 79, 104]. However, it is known that approximate DFT functionals might perform well for a specific property (e.g., for the frequently-used enthalpies of formation) and fail badly for other properties (e.g., for reaction barriers). For this study we chose the GMTKN30 database [107, 108] (1218 single point energies and 841 relative energy values) to identify further comfort zones of these new meta-GGAs. We also present new results that are outside of these comfort zones. Notice that these functionals were constructed by using exact constraints and no fitting to large molecular test sets was included in the design procedure.

GMTKN30 is a large main-group molecular energy test set composed of 30 smaller test sets and covers a large cross section of chemically relevant properties, and thus can give a comprehensive main-group molecular evaluation and assessment for a tested functional. Moreover, since all the popular density functionals have been tested by using GMTKN30, these results can be used to compare with those of the new meta-GGAs results. The GMTKN30 database involves decomposition energies, atomization energies, adiabatic ionization potentials, electron affinities, proton affinities, self-interaction-error related energies, reaction energy barrier heights, reaction energies, radical stabilization energies, isomerization energies, difficult systems for semi-local approximations, intramolecular dispersion energies, intermolecular noncovalent interaction energies, and conformational energies. The detailed description of the database can be found in Refs. [107, 108]. The reference geometries and energies are

available from the GMTKN30 website [109]. The reference energies are obtained from high-level calculations like W1, W4, CCSD(T)/CBS, and/or from experiment.

The computational details are explained in section II. In section III, we show results and discussions, where details of mean absolute errors of different functionals from the reference data for each individual subset are given and discussed. We also assess in section III the performances of different functionals with and without long-range dispersion corrections through the pair-wise potential approach.

## 4.2 Computation Details

We used the Gaussian 03 code [110] with new subroutines for revTPSS, and MGGA\_MS, which were implemented by us self-consistently. For non-self-consistent regTPSS calculations we used the self-consistent (SCF) revTPSS electron densities. Earlier results show that even LSDA electron densities can be successfully used for tests of the performance of various functionals, so it is expected that revTPSS electron densities give an excellent starting point for regTPSS calculations.

The basis set convergence was tested for the MB08\_165, DARC, and WATER27 subsets. In Table 8, comparisons between results from aug-cc-pVDZ, 6-311+G(3df,2p), aug-cc-pVTZ, and aug-cc-pVQZ basis sets show that the aug-cc-pVTZ basis set gives reasonable results with considerable efficiency. This latter TZ basis set is used for most of our calculations. Our results are in agreement with the conclusion in the literature [111] that the Kohn-Sham limit of semi-local functionals is almost reached with the (aug-)def2-TZVPP basis set, thus the expensive QZ basis sets are not necessary to test these

functionals. We used ‘fine grid’ (a pruned grid with 75 radial shells and 302 angular points per shell) for all calculations.

To account for scalar relativistic effects, Heavy28 and RG6 energies were calculated using the ECP-121G effective core potentials. The alkaline and alkaline-cation-benzene complexes were calculated using the 6-311++G basis set.

**Table 8** The mean absolute errors (kcal mol<sup>-1</sup>) of the basis sets compared to the basis-set limit for three smaller test sets using the revTPSS functional

Subset	aug-cc-pVDZ	6311+G(3df,2p)	aug-cc-pVTZ
MB08-165	1.8	1.2	0.3
DARC	4.7	1.0	0.1
WATER27	3.4	3.6	0.9

We have tested the functionals without but also with long-range dispersion corrections. Since geometries were fixed for all calculations, we extracted the D3 dispersion energy corrections from the published TPSS-D3 results [109] and used these corrections to correct the new meta-GGA results. The results of LSDA, PBE, M06L, and B3LYP are from the GMTKN30 website [109].

## 4.3 Results and Discussion

### 4.3.1 The Mean Absolute Errors

The mean absolute errors (MAEs) of the three new meta-GGA functionals - revTPSS, regTPSS, and MGGA-MS – for the 30 subsets of the GMTKN30 test set are compared with those of TPSS, PBE [34], M06L [44], and B3LYP [54, 55]. The latter two functionals are popular in molecular electronic structure calculations and this comparison is helpful for us to assess the overall performance of the new meta-GGAs. For the discussion we group the 30 subsets into three groups as suggested in the Ref. [111]. The



first group (or section) contains 8 subsets related to miscellaneous basic properties like decomposition energies, atomization energies, ionization potentials, electron affinities, proton affinities, self-interaction error related energies, and reaction energy barrier heights. This group or section was called basic properties in Ref. [111]. The second group contains 12 subsets related to chemical reaction energies like isomerizations, Diels–Alder reactions, ozonolyses, and reactions involving alkaline metals. The third group (the remaining 10 subsets) is related to non-covalent interactions and contains water clusters, conformational space energies, and systems with inter- and intramolecular London-dispersion interactions.

#### a. Miscellaneous Properties

Fig. 5 shows the MAEs of different functionals for eight subsets of the GMTKN30 test set related to miscellaneous basic properties. The “mindless benchmarking” or MB08-165 subset refers to the decomposition energies of 165 “artificial”, non-conventional, random-structure molecules into hydrides and diatomic homonuclear molecules. Fig. 5 shows that the MB08-165 subset is a difficult test for the present semi-local functionals and the largest errors occur here in the first group of the subsets. This can be attributed to the stretched structures where the non-locality of the electron hole is poorly described by the semi-local functionals. Inclusion of the exact exchange remedies the problem to some degree (Notice the slightly improved performance of PBE0 and TPSSh functionals for these test sets in Ref. [111]). Consequently the hybrid B3LYP gives the smallest MAE ( $8.2 \text{ kcal mol}^{-1}$ ) followed by PBE ( $\text{MAE}=9.0 \text{ kcal mol}^{-1}$ ). The calculated MAEs for TPSS, revTPSS, regTPSS, MGGA\_MS and M06L are 10.1, 15.8, 12.9, 17.5 and  $13.3 \text{ kcal mol}^{-1}$ , respectively. Notice from Ref. [111] that M06L does not converge for one of the decomposition energies, so its MAE cannot be evaluated

correctly. Like M05 [112], M06L has an oscillating enhancement factor that can cause a convergence problem [113], and no known convergence- improving technique can remedy this problem. The new meta-GGAs have no such problem. TPSS performs best among the tested meta-GGA functionals. An optimized TPSS (oTPSS) [111] (not shown in Fig 1) gives an MAE only 6.5 kcal mol<sup>-1</sup> and this shows that meta-GGA might give superior results over the more expensive hybrid functionals. oTPSS is an optimized functional that has the same form as TPSS. Seven TPSS parameters (not including the gradient coefficients for exchange) were fitted in a standard least-squares procedure [108]. Lifting all physical constraints, has a great influence on all seven parameter values. (For details see Table 5 of Ref. [108]). oTPSS gives the best meta-GGA results for this test. However such optimization to molecular test sets might lead to poor results in solid state applications. The accuracy of the heavily parameterized M06L (fitted to 350 energies) is worse than that of TPSS and regTPSS, but it is better than that of MGGA\_MS and revTPSS. Although both regTPSS and MGGA\_MS are free of the order-of-limits anomaly [58, 104] present in TPSS and revTPSS, their construction differences lead to different results for the MB08-165 subset.

The W4-08 subset contains the atomization energies of 99 small molecules. As B3LYP [54, 55] was parametrized to reproduce atomization energies and enthalpies of formation of small molecules it is not surprising that it gives the best results with MAE (4.3 kcal mol<sup>-1</sup>). For meta-GGAs, in this study the empirically fitted M06L delivers the best results, followed by TPSS, revTPSS, regTPSS and then MGGA\_MS. Literature data [111] shows that oTPSS shows the best meta-GGA performance (MAE=3.2 kcal mol<sup>-1</sup>). For this subset regTPSS gives only slightly (by 0.2 kcal mol<sup>-1</sup>) increased MAE compared

to its parent revTPSS functional. For this subset PBE gives poor results and the largest MAE (13 kcal mol<sup>-1</sup>). As described earlier [114], the PBE gives quite unbalanced molecular and heavy atomic energies and this error is corrected by TPSS and by all the new meta-GGAs efficiently. One important factor might be the one-electron self-interaction error freedom of the TPSS that gives improved atomization energies for molecules that contain H atoms. This will be discussed later (see discussions of PA and SIE11 subsets).

The next three subsets are G21IP, G21EA and PA, which represent the adiabatic ionization potentials, adiabatic electron affinities and adiabatic proton affinities, containing 36, 25, and 12 energies, respectively. The results in Fig. 5 show that all of the tested functionals give reasonable results for these three subsets. B3LYP shows the smallest MAE for the G21IP and the G21EA subsets and has an MAE comparable to that of PBE for the PA subset. At the basis-set limit, some negative ions are bound only when at least a fraction of exact exchange is included in the effective potential [115]. The overall performances of TPSS and revTPSS for these three subsets are better than regTPSS, MGGA\_MS and M06L. Notice that oTPSS shows a worse performance than TPSS for the G21IP and the G21EA subsets. For the PA subset, PBE works better than the meta-GGAs, and regTPSS and MGGA\_MS give large errors (cf. MAE = 7.3 and 7.8 kcal mol<sup>-1</sup>, respectively). For correct proton affinity results the accuracy of the total energy for the hydrogen atom is particularly important. PBE and TPSS give excellent total energy for the hydrogen atom and this is reflected in the good results. Although regTPSS and MGGA\_MS recover the exact exchange energy of the hydrogen atom, these

functionals have the one-electron self-correlation error that makes the total energy of one-electron regions slightly less accurate.

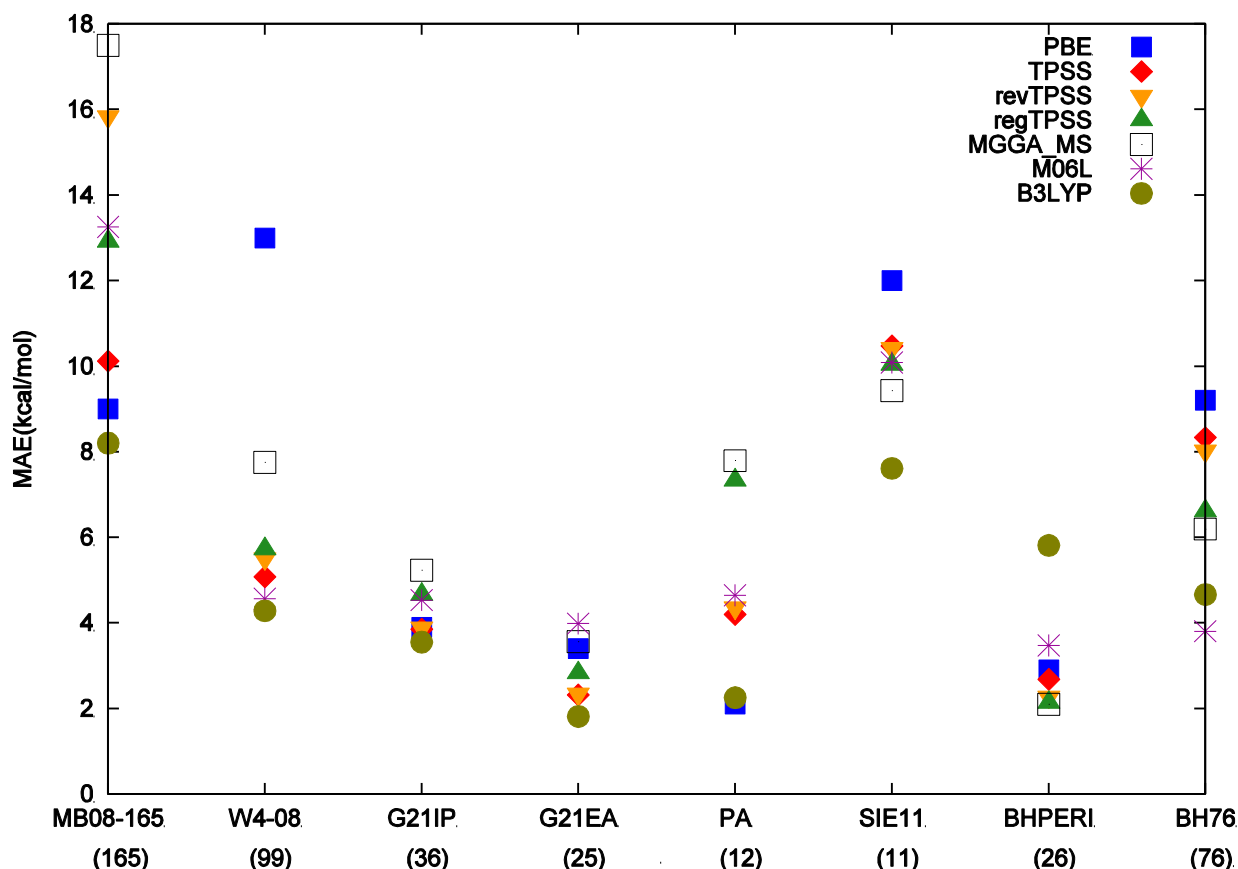


Fig. 5 MAEs of PBE, TPSS, revTPSS, regTPSS, MGGA\_MS, M06L and B3LYP for the eight subsets of the miscellaneous properties group in GMTKN30 database. A number under the name of a subset in a bracket indicates the number of entries of the subset.

The SIE11 subset includes 11 self-interaction related problems. The semi-local functionals are spoiled by one- and many-electron self-interaction error as described in the literatures [116, 117]. Fig. 5 shows that all studied functionals perform relatively poorly for this test set. The worst result is given by PBE (cf. Fig. 5, MAE=12 kcal mol<sup>-1</sup>). The meta-GGA functionals improve over PBE noticeably (cf. MAEs close to 10 kcal mol<sup>-1</sup>). Among the semi-local functionals, MGGA\_MS gives the smallest MAE=9.4 kcal mol<sup>-1</sup>. The B3LYP hybrid functional performs best (cf. MAE=7.6 kcal mol<sup>-1</sup>) as this

functional contains 25% exact exchange that decreases the electron self-interaction error for exchange and the LYP functional is one-electron self-correlation error free. But notice that the self-correlation error was reintroduced by the mixture of LSDA correlation into the correlation part of the functional. However, the overall balance of decrease and increase of the self-interaction errors helps B3LYP to decrease this error. Despite its optimization of the parameters, oTPSS gives only a negligible improvement over TPSS, as the many-electron self-interaction error cannot be corrected at the level of semi-local approximation.

The subsets BHPERI (26 barrier heights of pericyclic reactions) and BH76 (76 barrier heights of hydrogen transfer, heavy atom transfer, nucleophilic substitution, unimolecular and association reactions), test the performance for stretched-bond transition states. For the stretched bonds the correct description of electron hole delocalization is particularly difficult for the semi-local functionals. However, beside the similarities of the two tests, important differences exist. The BHPERI is the only subset in this miscellaneous group of subsets that also tests the noncovalent interactions classified in the third group. The 25% exact exchange helps B3LYP to describe better the electron hole delocalization effect and to give improved results for the BH76 test set. However this is not sufficient for BHPERI where the noncovalent interactions of the crowded ring structures are incorrectly described by the strongly repulsive B88 exchange functional. (Further proof of this is that the D3 noncovalent correction helps to bring down the large B3LYP error from almost 6 kcal mol<sup>-1</sup> to 2.8 kcal mol<sup>-1</sup>). Thus the uncorrected B3LYP shows the poorest performance for BHPERI. For BH76 where the noncovalent interactions are unimportant B3LYP shows the second best performance

after M06L. The good performance of the M06L is expected, as BH76 was in the training set of the parametrization of M06L, and M6L describes some part of the noncovalent interactions correctly. MGGA\_MS and regTPSS are better than TPSS and revTPSS with noticeable improvement on MAEs as shown in Fig. 5. Notice that oTPSS without long-range dispersion correction fails seriously for BHPERI ( $\text{MAE} = 4.6 \text{ kcal mol}^{-1}$ ) and gives considerably worse results than TPSS, while oTPSS-D3 performs well ( $\text{MAE} = 2.1 \text{ kcal mol}^{-1}$ ) [111] suggesting that the noncovalent interactions might be important for these energies. At this point it is interesting to note that revTPSS and regTPSS restore the second-order gradient expansion of a slowly-varying density for exchange over a wide range of densities like PBEsol, but PBEsol shows a poor performance for BHPERI ( $\text{MAE} = 6.9 \text{ kcal mol}^{-1}$ ) and this error is largely corrected by the more flexible revTPSS and regTPSS, showing the advantage of the meta-GGA formalism. Notice also that revPBE that performs well for molecular test sets fails for this test set ( $\text{MAE} = 4.2 \text{ kcal mol}^{-1}$ ).

#### b. Reaction Energies

Fig. 6 shows the MAEs of the studied functionals for twelve subsets in the GMTKN30 test set related to reaction energies. The first BH76RC subset includes the energies of 30 chemical reactions related to the previous BH76 subset. For the BH76RC subset, M06L gives the smallest MAE among the tested meta-GGAs, followed by TPSS, regTPSS, PBE, MGGA\_MS and revTPSS. There are only small differences between the semi-local functionals for this test set, and inclusion of the exact exchange is needed to improve the results (see improved B3LYP results). As published PBE with 25, 32,[118] and 38%[111] of exact exchange gives also very much improved results for this subset ( $\text{MAE} = 2.5 \pm 0.1 \text{ kcal mol}^{-1}$ ). The optimized oTPSS gives marginal improvements [111].

The RSE43 subset studies the stabilization energies of 43 radicals. As shown in Fig. 6 the meta-GGA functionals work better for this subset than PBE, which actually gives the largest MAE. As expected the inclusion of 25, 32 or 38% of exact exchange helps to bring down the MAE of PBE hybrid to  $1.5 \pm 0.3$  kcal mol<sup>-1</sup>. TPSS and M06L give similar MAEs of 3.0 kcal mol<sup>-1</sup> and 3.1 kcal mol<sup>-1</sup>, respectively. MGGA\_MS gives the best meta-GGA results (MAE = 2.0 kcal mol<sup>-1</sup>), followed by B3LYP, regTPSS, revTPSS, TPSS, M06L, and PBE.

The O3ADD6 subset is specifically designed for studying the reaction and association energies and barrier heights for addition of ozone (O<sub>3</sub>) to C<sub>2</sub>H<sub>4</sub> and C<sub>2</sub>H<sub>2</sub> molecules, and the G2RC subset describes 25 reaction energies for molecules selected from G2/97 test set. Fig. 6 shows that the best overall performance (MAE = 2.0 kcal mol<sup>-1</sup> for O3ADD6 and 2.6 kcal mol<sup>-1</sup> for G2RC) is achieved by B3LYP. Notice that B3LYP was optimized using the G2/97 test set. The meta-GGAs give MAE around 4 kcal mol<sup>-1</sup> for the O3ADD6 with small differences and M06L gives marginally better results than revTPSS. It is interesting that MGGA\_MS behaves very differently from the other meta-GGAs and gives a very large error for O3ADD6 and particularly for G2RC (MAE > 10 kcal mol<sup>-1</sup>). MGGA\_MS gives a larger error when single bonds are produced in a reaction. These poor MGGA\_MS results might be attributed to an excessive enhancement function for small  $s$  and  $\alpha$  regions. For the G2RC subset M06L, PBE and TPSS perform about the same and these functionals perform somewhat better than revTPSS and regTPSS. Notice that the empirical oTPSS gives a considerably better result (MAE = 3.5 kcal mol<sup>-1</sup>) only slightly worse than B3LYP.

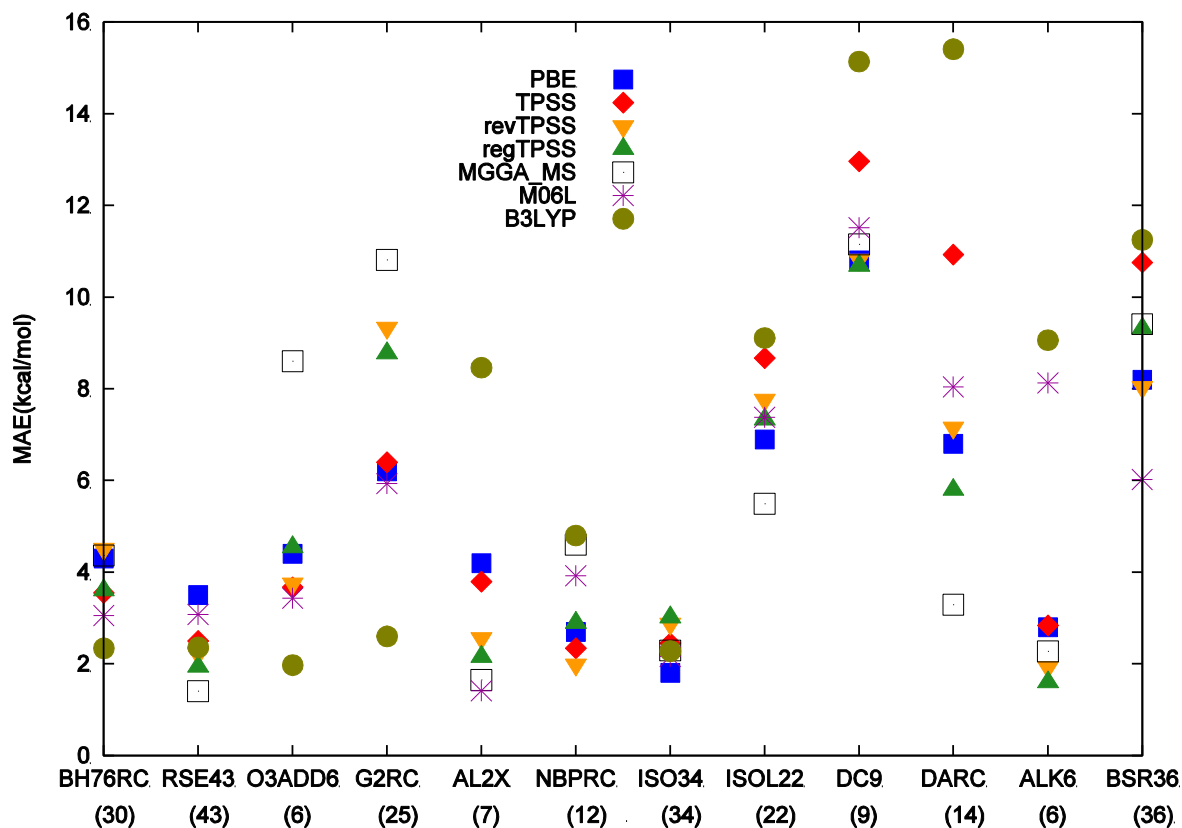


Fig. 6 MAEs of PBE, TPSS, revTPSS, regTPSS, MGGA\_MS, M06L and B3LYP for the reaction group in GMTKN30 database. A number under the name of a subset in a bracket indicates the number of entries of the subset.

The AL2X subset contains dimerization energies of  $\text{AlX}_3$  molecules, where  $X = \text{H}, \text{CH}_3, \text{F}, \text{Cl}, \text{Br}$  and the NBPRC subset contain oligomerization and  $\text{H}_2$  fragmentation energies of  $\text{NH}_3$  or  $\text{BH}_3$  molecules and  $\text{H}_2$  activation reactions with  $\text{PH}_3$  or  $\text{BH}_3$  molecules. For these reactions the correct description of noncovalent interactions again might give improved results. Fig. 6 shows that B3LYP that misses most of the noncovalent interaction energy and it performs particularly poorly for the AL2X, and also give the worst results for NBPRC reactions. All tested meta-GGA functionals are more suitable than B3LYP or PBE for calculating the AL2X subset, and M06L and MGGA\_MS give only slightly better results than revTPSS or regTPSS. For NBPRC



revTPSS gives the best results with  $\text{MAE} = 2.0 \text{ kcal mol}^{-1}$ , and M06L and MGGA\_MS show considerably poorer performance (MAEs around  $4 \text{ kcal mol}^{-1}$ ).

The next two subsets test the description of the isomerization energies. ISO34 contains isomerization energies of small and medium-sized organic molecules and ISOL22 contains isomerization energies large-sized organic molecules. The fundamental difference between the two test sets is that for large-sized molecules the correct description of the intra-molecular noncovalent interactions is important. For the ISO34 the B3LYP MAE of  $2.3 \text{ kcal mol}^{-1}$  is comparable to those of TPSS ( $2.5 \text{ kcal mol}^{-1}$ ), revTPSS ( $2.9 \text{ kcal mol}^{-1}$ ), MGGA\_MS ( $2.3 \text{ kcal mol}^{-1}$ ) and M06L ( $2.2 \text{ kcal mol}^{-1}$ ). PBE gives the best results for the ISO34 subset with an MAE of  $1.8 \text{ kcal mol}^{-1}$ . MGGA\_MS gives the best results for ISOL22.

ISOL22 apparently requires the correct description of intra-molecular noncovalent interactions. Notice that oTPSS gives very poor results for the ISOL22 reactions ( $\text{MAE} = 9.1 \text{ kcal mol}^{-1}$ ) and D3 correction helps to decrease this error to  $6.8 \text{ kcal mol}^{-1}$ . This shows clearly that noncovalent corrections might improve the meta-GGA results for ISOL22. MGGA\_MS gives the best meta-GGA results for ISOL22 ( $\text{MAE} = 5.5 \text{ kcal mol}^{-1}$ ).

The DC9 subset deals with nine difficult cases for density functional calculations. Fig. 6 shows that B3LYP gives the largest MAE of  $15.1 \text{ kcal mol}^{-1}$ . All the new meta-GGAs perform better than TPSS, although even those relatively good results are quite poor (MAEs around  $10 \text{ kcal mol}^{-1}$ ). For DC9 subset the inclusion of the noncovalent corrections might improve the result, as illustrated by the very poor oTPSS results (MAE

= 16.3 kcal mol<sup>-1</sup>) that are improved somewhat by D3 corrections (MAE = 12.8 kcal mol<sup>-1</sup>). The best new meta-GGAs for this are regTPSS and revTPSS.

The DARC subset includes 14 Diels-Alder reactions. For several of these reactions the ring structures provide some degree of intramolecular noncovalent interactions that are poorly described by B3LYP. Consequently B3LYP performs rather poorly for the DARC subset with MAE of 15.4 kcal mol<sup>-1</sup> (as it performs poorly for all subsets where noncovalent interactions play any role e.g. DC9, ISOL22, AL2X etc.). PBE gives better results for the DARC subset than TPSS (10.9 kcal mol<sup>-1</sup>), M06L (8.0 kcal mol<sup>-1</sup>), and revTPSS (7.2 kcal mol<sup>-1</sup>), but is worse than regTPSS (5.8 kcal mol<sup>-1</sup>). The smallest MAE is obtained by MGGA\_MS (3.3 kcal mol<sup>-1</sup>) as it includes some intramolecular interactions. The new meta-GGA functionals largely outperform the earlier meta-GGAs for the DARC.

The ALK6 subset contains chemical reactions of alkaline and alkaline-cation-benzene complexes. Fig. 6 shows that the performances of M06L (MAE = 8.1 kcal mol<sup>-1</sup>) and B3LYP (MAE = 9.1 kcal mol<sup>-1</sup>) are particularly poor for this subset. The new revTPSS and regTPSS give reasonably good performance (MAE < 2 kcal mol<sup>-1</sup>) and they are slightly better than TPSS and MGGA\_MS.

The BSR36 subset contains 36 bond separation reactions of saturated hydrocarbons. B3LYP again gives the largest MAE (11.3 kcal mol<sup>-1</sup>), as it does for ALK6, DARC and DC9 subsets. At the meta-GGA level, M06L performs the best while TPSS is the worst. revTPSS gives the best results among TPSS, revTPSS, regTPSS and MGGA\_MS. The calculated MAEs of regTPSS and MGGA\_MS are similar to each

other. For this subset the long-range dispersion corrections are very large for TPSS-type functionals (about 5.5 kcal mol<sup>-1</sup> improvement for MAE).

### c. Noncovalent Interactions

The weak dispersion interactions and hydrogen bonds are considered in the following six subsets: IDISP, WATER27, S22, ADIM6, RG6, and HEAVY28. In the WATER27 subset, hydrogen bonds between water molecules are dominant for the binding energies. The IDISP, ADIM6 and RG6 subsets require the correct description of the van der Waals interactions between molecules or atoms. Due to its long-range feature, the van der Waals interaction is believed to be difficult for a semi-local functional. However, results from the semi-local M06L, which was heavily fitted to a large number of training sets including noncovalent systems, suggest that a meta-GGA can capture medium-range exchange and correlation energies dominating noncovalent complexes [44]. Therefore, as expected M06L delivers the best overall performance for the six subsets while B3LYP is the worst among the tested functionals. But M06L is unable to bind the Kr<sub>2</sub> and Xe<sub>2</sub> dimers in RG6 and the PbH<sub>4</sub>-water and (TeH<sub>2</sub>)<sub>2</sub> complexes in HEAVY28 as observed earlier [111]. This together with a failure of M06L for MB08-165 requires caution when M06L is used for new problems. In this respect the new meta-GGAs are more robust, and we observed no similar problems. Although the nonempirical MGGA\_MS is inferior to M06L, it still yields quite good results for these subsets and systematically improves over the other semi-local functionals, among which TPSS captures the least noncovalent interactions. revTPSS and regTPSS show comparable

overall performances, which are slightly worse than that of PBE. But notice that for WATER27, where hydrogen bonds dominate binding energies, MGGA\_MS yields the smallest MAE, which is consistent with the finding for the W6 set of Ref. [58]. This confirms that MGGA\_MS describes the hydrogen bond excellently. Moreover, the quite good results for the other subsets from MGGA\_MS also corroborate the findings from the semi-local M06L that equilibrium structures of noncovalent complexes are dominated by medium-range exchange and correlation energies, which a meta-GGA is able to describe at least partly. Without long-range dispersion correction, no TPSS-type meta-GGA can perform reasonably for IDISP, Water27, S22, and ADIM6.

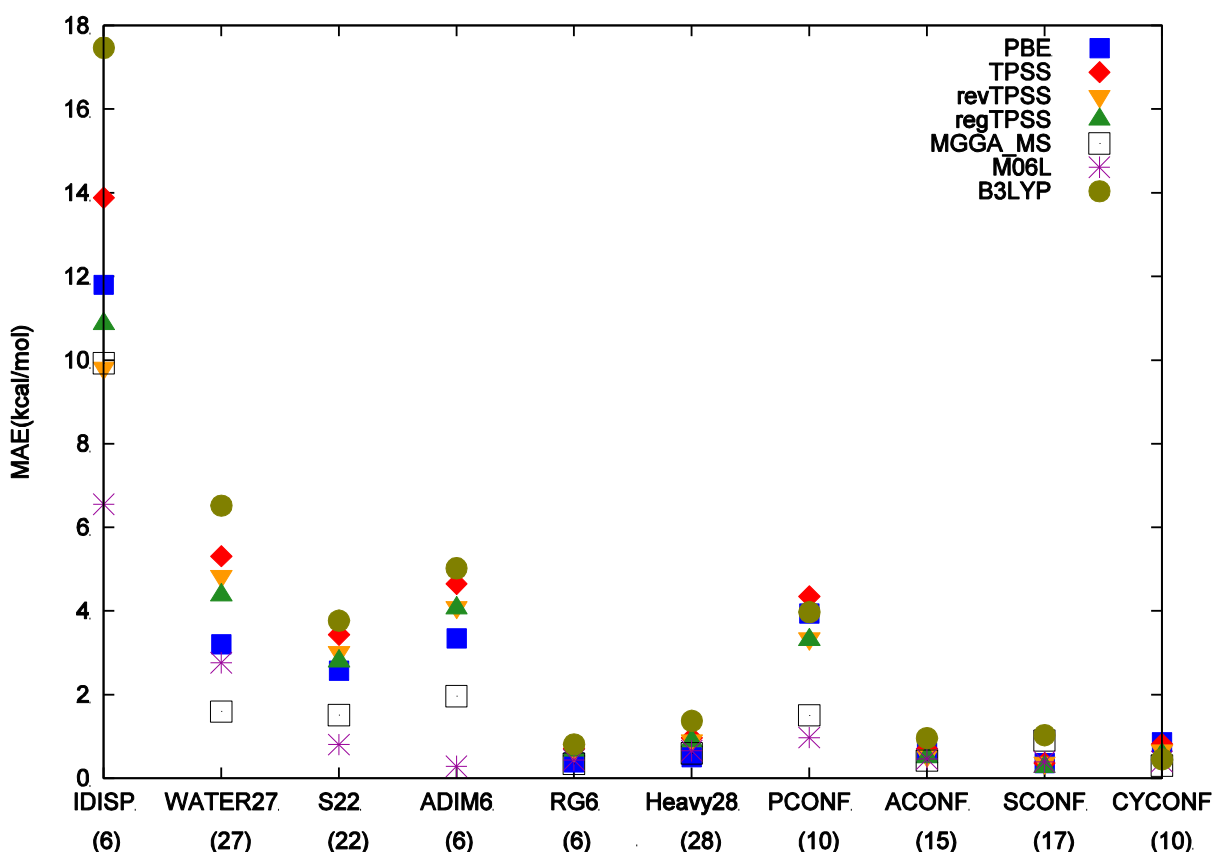


Fig. 7 MAEs of PBE, TPSS, revTPSS, regTPSS, MGGA\_MS, M06L and B3LYP for the noncovalent interaction group in GMTKN30 database. A number under the name of a subset in a bracket indicates the number of entries of the subset.

The last four subsets are PCONF, ACONF, SCONF and CYCONF. These four subsets are related to the relative energies of different conformers of molecules. The transformation between different conformers is usually associated with the change of chemical bonds. The results of MAEs are given in Fig. 7. For the PCONF the noncovalent energy contributions are particularly large, consequently M06L performs the best (1.0 kcal mol<sup>-1</sup>), followed by MGGA\_MS (1.5 kcal mol<sup>-1</sup>), regTPSS (3.3 kcal mol<sup>-1</sup>), revTPSS (3.4 kcal mol<sup>-1</sup>), PBE (3.9 kcal mol<sup>-1</sup>), B3LYP (4.0 kcal mol<sup>-1</sup>), and TPSS (4.4 kcal mol<sup>-1</sup>). For the other three subsets, the overall performances of the tested functionals are close to each other. B3LYP is the least accurate and the meta-GGAs give somewhat worse result than PBE.

### 4.3.2 Weighted Total Mean Absolute Error

We use the weighted total mean absolute error (WTMAE) defined by Goerigk and Grimme [111], as  $\frac{\sum_i W_i \text{MAE}_i}{\sum_i W_i}$ , where  $W_i$  and  $\text{MAE}_i$  are the weight and MAE for the subset  $i$  (see the definition of  $W_i$  from Ref. [111]). To keep the analysis consistent with previous work, we use this definition of weight for each subset. However, because the MB08-165 subset consists of “artificial” reactions which have a large weight, and an assessment of density functionals based on this subset might not be indicative for “real” chemical reactions. So we shall report the WTMAE without as well as with the MB08-165 subset. While the exact density functional should describe MB08-165, the meta-GGAs may fail there because of the high level of strain in the artificial complexes. Table 9 shows the MAE of the MB08-165 subset, the WTMAEs of the miscellaneous properties and the

total GMTKN30 database with and without the MB08-165 subset, and the WTMAEs of the reaction energies and the noncovalent bonds. Considering miscellaneous properties and the total test set, if we exclude the MB08-165 subset, there is a little change for PBE but for meta-GGAs, particularly for revTPSS, regTPSS, and MGGA\_MS, the change is considerable. The large weight of the performance for the “artificial” MB08-165 (37.6% of the 8 miscellaneous properties’ subsets and 14.4% of the total 30 weights) hides considerably the reasonable performance of meta-GGAs for “real” chemical reactions. So we exclude the MB08-165 subset for later discussion.

**Table 9** The MAE or WTMAE of the discussed functionals for the MB08-165 subset, the miscellaneous properties group, the reaction energies, the noncovalent bonds and the total test set. <sup>a</sup>

	LSDA	PBE	TPSS	revTPSS	regTPSS	MGGA_MS	M06L	B3LYP
MB08-165 <sup>b</sup>	20.3	9.0	10.1	15.8	12.9	17.5	13.3	8.2
Misc. Properties(7) <sup>c</sup>	22.5	8.3	5.5	5.5	5.3	5.9	4.3	4.4
Misc. Properties(8) <sup>d</sup>	21.7	8.5	7.2	9.4	8.1	10.2	7.7	5.8
Reaction Energies (12) <sup>e</sup>	6.9	5.5	6.5	5.6	5.6	5.5	5.0	7.1
Noncovalent Bonds(10) <sup>f</sup>	4.9	2.9	3.7	3.0	2.9	1.9	1.3	4.2
Total(29) <sup>g</sup>	10.5	5.4	5.2	4.7	4.6	4.3	3.5	5.3
Total (30) <sup>h</sup>	11.9	5.9	5.9	6.3	5.8	6.2	4.9	5.8

<sup>a</sup> Unit is in kcal mol<sup>-1</sup>. The values in the parentheses are the number of subsets. <sup>b</sup> The MAE of the MB08-165. <sup>c</sup> The WTMAE of the miscellaneous properties subgroup that excludes the MB08-165 subset. <sup>d</sup> The WTMAE of the miscellaneous properties subgroup that includes the MB08-165 subset. <sup>e</sup> The WTMAE of the reaction energies subgroup. <sup>f</sup> The WTMAE of the noncovalent bonds subgroup. <sup>g</sup> The WTMAE of the total GMTKN database that includes the MB08-165 subset. <sup>h</sup> The WTMAE of the total GMTKN database that excludes the MB08-165 subset.

The LSDA[10] in the SPW92 parametrization [22] is included in Table 9, using the data from Ref. [109, 111]. LSDA works the worst for the total 29 subsets. It

especially delivers much larger WTMAE for miscellaneous properties, and its overbinding yields a bad performance for noncovalent interactions, which cannot be corrected by long-range dispersion. M06L delivers the best performance for these three groups separately or together in terms of WTMAE. B3LYP works well for miscellaneous properties but yields the largest WTMAE for the reaction energies and noncovalent interactions except SVWN. While the three new meta-GGAs (revTPSS, regTPSS, and MGGA\_MS) have similar performance on miscellaneous properties and reaction energies, MGGA\_MS outperforms the other two for the noncovalent interactions. For the 29 subsets, B3LYP, PBE and TPSS have larger WTMAEs than those of the three new meta-GGAs.

### 4.3.3 Results with the Dispersion Correction

As we know the long-range correlation interaction decays exponentially for semi-local functionals [119] arising only from the density overlap region, while the true van der Waals interaction decays as of  $R^{-6}$  for objects separated by a large distance  $R$ . Therefore, semi-local density functionals cannot capture long-range correlation energy for van der Waals interactions [120]. The DFT-D approach is a very quick simple way to compensate the missing dispersion energy [121], which treats the dispersion energy as a post hoc correction to a semi-local functional.

One possible formula for the long-range dispersion interactions that decays as  $R^{-6}$  is:

$$E_{disp} = -\frac{1}{2} \sum_{A \neq B} \sum_{n=6,8} S_n \frac{C_n^{AB}}{R_{AB}^n} f_{damp,n}(R_{AB}), \quad (4-1)$$

where  $C_n^{AB}$  is the averaged  $n^{\text{th}}$ -order van der Waals coefficient for the pair of atoms A and B, and  $R_{AB}$  is the separation between the two atoms.  $S_n$  is a scaling factor for the  $n^{\text{th}}$ -order dispersion energy. In the DFT-D3 version,  $S_6$  is equal to unity and  $S_8$  is adjusted specifically for a given functional [111].  $f_{damp,n}(R_{AB})$  is a damping function that is used to remove the energy singularity for small R and the double counting of the correlation at intermediate range. The damping function involves a functional-dependent parameter  $S_{r,n}$ , which is a scaling factor for the cutoff radius. This cutoff radius usually refers to the van der Waals radius [122], but in DFT-D3, it is derived from the average atomic radius [121]. For DFT-D3,  $S_{r,8}$  is equal to unity and  $S_{r,6}$  is dependent on the specific functional [111]. Decreasing  $S_n$  or increasing  $S_{r,n}$  can reduce the dispersion energy. For the three new meta-GGAs, their optimized damping functions are not known yet. We used the TPSS-D3 dispersion energy to correct these new functionals as described in the Sec II.

**Table 10** The WTMAE of the discussed functionals for different test sets with D3 correction in kcal mol<sup>-1</sup>. The D3 corrections for revTPSS, regTPSS, and MGGA\_MS are those designed for TPSS, and are not optimal for other functionals, especially MGGA\_MS.

	PBE	TPSS	revTPSS	regTPSS	MGGA_MS	M06L	B3LYP
Misc. Properties(7) <sup>a</sup>	8.6	5.8	6.0	5.8	6.4	4.3	4.1
Misc. Properties(8) <sup>b</sup>	8.8	7.2	9.4	8.0	10.3	7.6	5.0
Reaction Energies	4.3	4.6	4.0	4.2	4.8	4.9	4.7
Noncovalent Bonds	1.6	1.2	1.2	1.2	2.2	1.2	1.1
Total (29) <sup>a</sup>	4.5	3.8	3.6	3.6	4.3	3.4	3.3
Total (30) <sup>b</sup>	5.2	4.6	5.2	4.7	6.1	4.8	3.7

<sup>a</sup> The subset MB08-165 is excluded. <sup>b</sup> The subset MB08-165 is included.



Table 10 shows that the inclusion of the TPSS-D3 dispersion energy largely improves WTMAEs of regTPSS and revTPSS for the noncovalent interactions to the same level of TPSS-D3, but deteriorates MGGA\_MS slightly. This suggests that TPSS, revTPSS, and regTPSS miss a large portion of noncovalent interactions, but MGGA\_MS behaves very differently (it is more overbinding than regTPSS or revTPSS). Addition of long-range dispersion binding to an already correct or overbinding result naturally worsens the result as it increases the overbinding. The inclusion of the TPSS-D3 dispersion energy causes double counting of the part of noncovalent interactions captured by MGGA\_MS and thus deteriorates its performance with increasing the noncovalent WTMAE from 1.9 kcal mol<sup>-1</sup> to 2.2 kcal mol<sup>-1</sup>. If we correct MGGA\_MS by using the M06L-D3 dispersion energy correction - which has a smaller dispersion energy correction with  $S_{r,6}=1.581$  and  $S_8=0$  with practically no correction for the MAE - the WTMAE for the noncovalent reactions is improved from 1.9 kcal mol<sup>-1</sup> to 1.6 kcal mol<sup>-1</sup>. The inclusion of the dispersion corrections also improves the performances of all the tested functionals for the reaction energies, but deteriorates those for the miscellaneous basic properties (e.g., reaction barrier heights). Otherwise, B3LYP-D3 yields the smallest WTMAE for the total 29 subsets. revTPSS-D3 and regTPSS-D3 also give quite good results for the total 29 subsets with the WTMAEs only 0.3 kcal mol<sup>-1</sup> larger than that of M06L. revTPSS-D3 even gives the smallest WTMAE for the reaction energies among all tested functionals. As it does not use a properly fitted D3 correction, some improvement is possible, mostly for the worsened miscellaneous energies.

## 4.4 Conclusion and Summary

We have tested the nonempirical semi-local meta-GGAs, i.e., TPSS, revTPSS, regTPSS, and MGGA\_MS on the GMTKN30 molecular database for a variety of properties, some of which (for example, barrier heights and noncovalent interactions) are difficult for semi-local functionals. For comparison, we also included results of PBE, M06L, and B3LYP from the literature [111]. While revTPSS and regTPSS are comparable to each other overall, MGGA\_MS, when compared to them, is slightly worse for miscellaneous properties, comparable for reaction energy, and systematically better for noncovalent interactions. For miscellaneous properties, these three meta-GGAs perform in general much better than PBE, and not as well as M06L and B3LYP. For kinetic properties, B3LYP surprisingly delivers the worst overall performance, and TPSS performs the second worst, while the other functionals perform better with accuracy similar to each other. For noncovalent interactions, B3LYP is again the worst one and M06L performs the best. MGGA\_MS is the second best one, which shows large improvement on noncovalent interactions (stronger binding) over PBE, TPSS, revTPSS, and regTPSS. The latter functionals are at the same accuracy level and can be significantly improved by the inclusion of the dispersion correction for this category. The quite good performances of MGGA\_MS and M06L, compared to those of the other semi-local functionals without long-range dispersion corrections, suggest that equilibrium structures of noncovalent complexes are dominated by medium-range van der Waals interactions which then can be described at least partly by semi-local meta-GGAs.

The density functionals tested here for main-group chemical energetics achieve a similar overall accuracy. So what are the take-home lessons for users and developers?

The first is that no density functional yet comes close to the desired chemical accuracy (mean absolute error of 1 kcal mol<sup>-1</sup>), but all of those tested achieve a useful accuracy. Moreover, the tested semi-local functionals (PBE GGA and the meta-GGAs) are more computationally efficient for large molecules than is the hybrid functional B3LYP.

The second is that for some individual data subsets there is a wide range of mean absolute errors among these functionals. A dramatic example is the DARC subset of 14 Diels-Alder reaction energies, where the mean absolute error is 3 kcal mol<sup>-1</sup> for MGGA\_MS but 15 kcal mol<sup>-1</sup> for B3LYP. This suggests that, for a specific application, the user can sometimes choose a functional that is expected to work best.

The Diels-Alder reactions (DARC) and the dimerization of aluminum complexes (AL2X) involve the formation of rings and the reaction energies are influenced by noncovalent interactions. They have been discussed as difficult cases for approximate functionals [123]. For both, B3LYP is the worst performer and MGGA-MS is the best or nearly the best. But this order of performance is reversed in the reaction subsets BH76RC, O3ADD6, and G2RC. More generally, the standard B3LYP is outperformed by the tested semi-local functionals for data sets dominated by ring structures (DARC, AL2X, BHPERI, DC9). But notice that B3LYP has the worst MAD of all hybrids [111]. Interestingly, the originally suggested B3PW91-D3 is one of the best functional. Among the conventional hybrids PW6B95-D3 gives the best results for GMTKN30 and it is

somewhat outperformed by the non-conventional, heavily fitted M06-2X-D3 dispersion corrected meta-GGA hybrid (but naturally the same convergence problems hold for M06L and M06-2X [113]). The new meta-GGAs perform better than the older ones for several subsets. revTPSS is the best or very close to be the best for 15 subsets, namely G21IP, G21EA, BHPERI, NBPRC, ISOL22, DC9, BSR36, ALK6, BSR36, IDISP, S22, RG6, PCONF, ACONF, SCONF. For BHPERI, ALK6, and SCONF, revTPSS is marginally beaten by regTPSS. MGAA\_MS is the best or almost the best for 7 subsets: SIE11, BHPERI, RS43, AL2X, ISOL22, WATER27, and CYCONF. There is a very delicate question what to do when the D3 correction worsens the results of functionals that were constructed on the basis of the exact constraints. For example, in the BHPERI and BH76 subgroups the barrier height is typically underestimated. Adding D3 shifts the results in the wrong direction for many functionals (oTPSS, TPSS). Worsening the results this way might be consistent, but hard to accept.

The third is that, if one seeks an overall-best functional, then one must identify or develop candidates beyond the current meta-GGAs and B3LYP hybrid studied here, or look for criteria beyond main-group chemical energetics. Indeed, some of the hybrid functionals studied in Ref. [111], with dispersion corrections, do perform somewhat better overall than the functionals in our Table 10. And there may be much room for further improvement of meta-GGA and hybrid meta-GGA functionals. Savin and collaborators [124, 125] have proposed that currently the selection of a functional is largely a personal choice, like the selection of a spouse. They have also shown how different statistical measures on the same data set can lead to different conclusions about the relative performance of approximate functionals.

A formal criterion is the extent to which the approximation was constructed from exact constraints on the density functional for the exchange-correlation energy (as in PBE, TPSS, revTPSS, regTPSS, and MGGA\_MS), and not from fitting to experimental (as in M06L and B3LYP) or calculated high-level reference data.

A "universality" criterion would be the applicability of the functional for non-main-group chemistry as well as for solids, solid surfaces, and molecules on surfaces, where revTPSS has shown promise [88], as have (at least for bulk solids) highly empirical functionals [126] fitted to solid state as well as chemical data.

While this chapter reports only error statistics, the individual energy differences and their errors are available as supplementary information.

## References

- [1] M. Born and J. R. Oppenheimer, *Ann. Physik* **84**, 457 (1927).
- [2] A. Szabo and N. S. Ostlund, *Modern Quantum Chemistry* (MacMillan, New York, 1982).
- [3] M. Headgordon, J. A. Pople, and M. J. Frisch, *Chem. Phys. Lett.* **153**, 503 (1988).
- [4] J. A. Pople, R. Seeger, and R. Krishnan, *Int. J. Quantum Chem.* **12 (S11)**, 149 (1977).
- [5] J. A. Pople, J. S. Binkley, and R. Seeger, *Int. J. Quantum Chem.* **10 (S10)**, 1 (1976).
- [6] P. Fulde, *Electron correlations in molecules and solids* (Springer, Berlin, 1993).

- [7] D. M. Ceperley and B. J. Alder, Phys. Rev. Lett. **45**, 566 (1980).
- [8] J. P. Perdew and S. Kurth, *A primer in density functional theory*, edited by C. Fiolhais, F. Nogueira and M. A. L. Marques (Springer-verlag, Berlin, 2003), p. 1-53.
- [9] P. Hohenberg and W. Kohn, Phys. Rev. **136**, B864 (1964).
- [10] W. Kohn and L. J. Sham, Phys. Rev. **140**, A1133 (1965).
- [11] S. Baroni, S. de Gironcoli, A. Dal Corso, and P. Giannozzi, Rev. Mod. Phys. **73**, 515 (2001).
- [12] R. G. Parr and W. Yang, *Density Functional Theory of Atoms and Molecules* (Oxford University Press, 1989).
- [13] M. Levy, Proc. Natl. Acad. Sci. U. S. A. **76**, 6062 (1979).
- [14] D. C. Langreth and J. P. Perdew, Solid State Commun. **17**, 1425 (1975).
- [15] O. Gunnarsson and B. I. Lundqvist, Phys. Rev. B **13**, 4274 (1976).
- [16] J. P. Perdew and S. Kurth, *Density functionals: Theory and application* (Springer, Berlin, 1996).
- [17] G. L. Oliver and J. P. Perdew, Phys. Rev. A **20**, 397 (1979).
- [18] N. W. Ashcroft and N. D. Mermin, *Solid state physics* (Holt, Rinehart, and Winston, New York, 1976).
- [19] M. Gell-Mann and K. A. Brueckner, Phys. Rev. **106**, 364 (1957).
- [20] L. Onsager, L. Mittag, and M. Stephen, Ann. Phys. (Leipzig) **18**, 71 (1966).
- [21] R. A. Coldwell-Horsfall and A. A. Maradudin, J. Math. Phys. **1**, 395 (1960).
- [22] J. P. Perdew and Y. Wang, Phys. Rev. B **45**, 13244 (1992).
- [23] S. H. Vosko, L. Wilk, and M. Nusair, Can. J. Phys. **58**, 1200 (1980).

- [24] P. S. Svendsen and U. vonBarth, Phys. Rev. B **54**, 17402 (1996).
- [25] D. J. W. Geldart and M. Rasolt, Phys. Rev. B **13**, 1477 (1976).
- [26] D. C. Langreth and J. P. Perdew, Phys. Rev. B **21**, 5469 (1980).
- [27] Y. Wang and J. P. Perdew, Phys. Rev. B **43**, 8911 (1991).
- [28] S. K. Ma and K. A. Brueckner, Phys. Rev. **165**, 18 (1968).
- [29] J. P. Perdew, Phys. Rev. Lett. **55**, 1665 (1985).
- [30] J. P. Perdew, *Electronic Structure of Solids '91*, edited by P. Ziesche and H. Eschrig, (Akademie Verlag, Berlin, 1991), p. 11.
- [31] J. P. Perdew, K. Burke, and Y. Wang, Phys. Rev. B **54**, 16533 (1996).
- [32] J. P. Perdew, Phys. Rev. B **33**, 8822 (1986).
- [33] J. P. Perdew and W. Yue, Phys. Rev. B **33**, 8800 (1986).
- [34] J. P. Perdew, K. Burke, and M. Ernzerhof, Phys. Rev. Lett. **77**, 3865 (1996).
- [35] D. C. Langreth and M. J. Mehl, Phys. Rev. B **28**, 1809 (1983).
- [36] C. T. Lee, W. T. Yang, and R. G. Parr, Phys. Rev. B **37**, 785 (1988).
- [37] B. Hammer, L. B. Hansen, and J. K. Norskov, Phys. Rev. B **59**, 7413 (1999).
- [38] A. D. Becke, Phys. Rev. A **38**, 3098 (1988).
- [39] A. D. Becke, J. Chem. Phys. **88**, 1053 (1988).
- [40] S. N. Steinmann, G. Csonka, and C. Corminboeuf, J. Chem. Theory Comput. **5**, 2950 (2009).
- [41] J. P. Perdew, A. Ruzsinszky, G. I. Csonka, O. A. Vydrov, G. E. Scuseria, L. A. Constantin, X. Zhou, and K. Burke, Phys. Rev. Lett. **100**, 136406 (2008).
- [42] T. Van Voorhis and G. E. Scuseria, J. Chem. Phys. **109**, 400 (1998).
- [43] M. Ernzerhof and G. Scuseria, J. Chem. Phys. **111**, 911 (1999).

- [44] Y. Zhao and D. G. Truhlar, J. Chem. Phys. **125**, 194101 (2006).
- [45] Y. Zhao and D. G. Truhlar, J. Chem. Phys. **128**, 184109 (2008).
- [46] J. P. Perdew, S. Kurth, A. Zupan, and P. Blaha, Phys. Rev. Lett. **82**, 2544 (1999).
- [47] J. Tao, J. P. Perdew, V. N. Staroverov, and G. E. Scuseria, Phys. Rev. Lett. **91**, 146401 (2003).
- [48] J. P. Perdew, A. Ruzsinszky, G. I. Csonka, L. A. Constantin, and J. Sun, Phys. Rev. Lett. **103**, 026403 (2009).
- [49] A. D. Becke and M. R. Roussel, Phys. Rev. A **39**, 3761 (1989).
- [50] A. D. Becke, J. Comput. Chem. **20**, 63 (1999).
- [51] V. N. Staroverov, G. E. Scuseria, J. M. Tao, and J. P. Perdew, J. Chem. Phys. **119**, 12129 (2003).
- [52] J. P. Perdew and K. Schmidt, *Density Functional Theory and Its Application to Materials*, edited by V. E. van Doren, C. van Alsenoy and P. Geerlings (American Institute of Physics, AIP Conference Proceedings Vol. 577, 2001).
- [53] A. D. Becke, J. Chem. Phys. **98**, 1372 (1993).
- [54] A. D. Becke, J. Chem. Phys. **98**, 5648 (1993).
- [55] P. J. Stephens, F. J. Devlin, C. F. Chabalowski, and M. J. Frisch, J. Phys. Chem. **98**, 11623 (1994).
- [56] J. M. Pitarke and A. G. Eguiluz, Phys. Rev. B **63**, 045116 (2001).
- [57] J. Harl and G. Kresse, Phys. Rev. Lett. **103**, 056401 (2009).
- [58] J. Sun, B. Xiao, and A. Ruzsinszky, J. Chem. Phys. **137**, 051101 (2012).
- [59] A. Messiah, *Quantum Mechanics* (North-Holland, Amsterdam, 1962), p. 686.



- [60] W. H. Press, S. A. Teukolsky, W. T. Vetterling, and B. P. Flannery, *Numerical Recipes: The Art of Scientific Computing* (Cambridge University Press, Cambridge, U.K., 1989).
- [61] I. Stich, R. Car, M. Parrinello, and S. Baroni, Phys. Rev. B **39**, 4997 (1989).
- [62] M. C. Payne, M. P. Teter, D. C. Allan, T. A. Arias, and J. D. Joannopoulos, Rev. Mod. Phys. **64**, 1045 (1992).
- [63] Y. Saad and M. H. Schultz, SIAM (Soc. Ind. Appl. Math. ) J. Sci. Stat. Comput. **7**, 856 (1986).
- [64] G. D. Mahan, Phys. Rev. A **22**, 1780 (1980).
- [65] P. D. De Cicco and F. A. Johnson, Proc. R. Soc. Lond. A **310**, 111 (1969).
- [66] R. M. Pick, M. H. Cohen, and R. M. Martin, Phys. Rev. B **1**, 910 (1970).
- [67] G. Kresse and J. Hafner, Phys. Rev. B **47**, 558 (1993).
- [68] G. Kresse and J. Hafner, Phys. Rev. B **49**, 14251 (1994).
- [69] G. Kresse and J. Furthmuller, Comput. Mat. Sci. **6**, 15 (1996).
- [70] G. Kresse and J. Furthmuller, Phys. Rev. B **54**, 11169 (1996).
- [71] P. Giannozzi, S. Baroni, N. Bonini, *et al*, J. Phys. Condens. Matter **21**, 395502 (2009).
- [72] G. T. Velde and E. J. Baerends, Physical Review B **44**, 7888 (1991).
- [73] G. Wiesenekker and E. J. Baerends, *Quadratic integration over the three-dimensional Brillouin zone*, 1991), 3, p. 6721.
- [74] BAND2010, SCM, Theoretical Chemistry, Vrije Universiteit, Amsterdam, The Netherlands, <http://www.scm.com>.

- [75] P. Hao, Y. Fang, J. Sun, G. I. Csonka, P. H. T. Philipsen, and J. P. Perdew, Physical Review B **85**, 014111 (2012).
- [76] R. M. Martin, *electronic structure* (Cambridge University Press, New York, 2004).
- [77] J. P. Perdew, V. N. Staroverov, J. Tao, and G. E. Scuseria, Phys. Rev. A **78**, 052513 (2008).
- [78] J. P. Perdew, K. Burke, and M. Ernzerhof, Phys. Rev. Lett. **77**, 3865 (1996).
- [79] J. Tao, J. P. Perdew, V. N. Staroverov, and G. E. Scuseria, Phys. Rev. Lett. **91**, 146401 (2003).
- [80] A. E. Mattsson, R. Armiento, and T. R. Mattsson, Phys. Rev. Lett. **101**, 239701 (2008).
- [81] J. P. Perdew, A. Ruzsinszky, G. I. Csonka, O. A. Vydrov, G. E. Scuseria, L. A. Constantin, X. Zhou, and K. Burke, Phys. Rev. Lett. **101**, 239702 (2008).
- [82] G. I. Csonka, O. A. Vydrov, G. E. Scuseria, A. Ruzsinszky, and J. P. Perdew, J. Chem. Phys. **126**, 244107 (2007).
- [83] A. B. Alchagirov, J. P. Perdew, J. C. Boettger, R. C. Albers, and C. Fiolhais, Phys. Rev. B **63**, 224115 (2001).
- [84] V. N. Staroverov, G. E. Scuseria, J. Tao, and J. P. Perdew, Phys. Rev. B **69**, 075102 (2004).
- [85] G. I. Csonka, J. P. Perdew, A. Ruzsinszky, P. H. T. Philipsen, S. Lebegue, J. Paier, O. A. Vydrov, and J. G. Angyan, Phys. Rev. B **79**, 155107 (2009).
- [86] P. Haas, F. Tran, and P. Blaha, Phys. Rev. B **79**, 085104 (2009).

- [87] P. Haas, F. Tran, P. Blaha, L. S. Pedroza, A. J. R. da Silva, M. M. Odashima, and K. Capelle, Phys. Rev. B **81**, 125136 (2010).
- [88] J. Sun, M. Marsman, A. Ruzsinszky, G. Kresse, and J. P. Perdew, Phys. Rev. B **83**, 121410 (2011).
- [89] B. B. Karki, R. M. Wentzcovitch, S. de Gironcoli, and S. Baroni, Phys. Rev. B **61**, 8793 (2000).
- [90] L. Schimka, J. Harl, and G. Kresse, J. Chem. Phys. **134**, 024116 (2011).
- [91] J. S. Dugdale and D. K. C. MacDonald, Phys. Rev. **89**, 832 (1953).
- [92] [www.quantum-espresso.org](http://www.quantum-espresso.org), (2010).
- [93] V. I. Ivashchenko and P. E. A. Turchi, Phys. Rev. B **78**, 224113 (2008).
- [94] R. Neumann, R. H. Nobes, and N. C. Handy, Mol. Phys. **87**, 1 (1996).
- [95] J. Tao, J. P. Perdew, and A. Ruzsinszky, Phys. Rev. B **81**, 233102 (2010).
- [96] J. Sun, M. Marsman, G. I. Csonka, A. Ruzsinszky, P. Hao, Y. Kim, G. Kresse, and J. P. Perdew, Phys. Rev. B **84**, 035117 (2011).
- [97] P. Hao, J. Sun, B. Xiao, A. Ruzsinszky, G. Csonka, J. Tao, S. Glindmeyer, and J. P. Perdew, J. Chem. Theory Comput. DOI: 10.1021/ct300868x (2012).
- [98] J. P. Perdew, J. A. Chevary, S. H. Vosko, K. A. Jackson, M. R. Pederson, D. J. Singh, and C. Fiolhais, Phys. Rev. B **46**, 6671 (1992).
- [99] M. Dion, H. Rydberg, E. Schröder, D. C. Langreth, and B. I. Lundqvist, Phys. Rev. Lett. **92**, 246401 (2004).
- [100] J. Sun, J. P. Perdew, and M. Seidl, Phys. Rev. B **81**, 085123 (2010).
- [101] R. Armiento and A. Mattsson, Phys. Rev. B **72**, 085108 (2005).
- [102] P. Haas, F. Tran, P. Blaha, and K. Schwarz, Phys. Rev. B **83**, 205117 (2011).

- [103] A. Vela, V. Medel, and S. B. Trickey, *J. Chem. Phys.* **130**, 244103 (2009).
- [104] A. Ruzsinszky, J. Sun, B. Xiao, and G. I. Csonka, *J. Chem. Theory Comput.* **8**, 2078 (2012).
- [105] J. P. Perdew, J. Tao, V. N. Staroverov, and G. E. Scuseria, *J. Chem. Phys.* **120**, 6898 (2004).
- [106] G. I. Csonka, A. Ruzsinszky, and J. P. Perdew, *J. Phys. Chem. B* **109**, 21471 (2005).
- [107] L. Goerigk and S. Grimme, *J. Chem. Theory Comput.* **7**, 291 (2011).
- [108] L. Goerigk and S. Grimme, *J. Chem. Theory Comput.* **6**, 107 (2010).
- [109] <http://toc.uni-muenster.de/GMTKN/GMTKN30/GMTKN30main.html>.
- [110] M. J. Frisch, G. W. Trucks, H. B. Schlegel, *et al*, Gaussian 03 code.
- [111] L. Goerigk and S. Grimme, *Phys. Chem. Chem. Phys.* **13**, 6670 (2011).
- [112] Y. Zhao, N. E. Schultz, and D. G. Truhlar, *J. Chem. Theory Comput.* **2**, 364 (2006).
- [113] G. I. Csonka, A. D. French, G. P. Johnson, and C. A. Stortz, *J. Chem. Theory Comput.* **5**, 679 (2009).
- [114] G. Csonka, A. Ruzsinszky, J. Tao, and J. Perdew, *Int. J. Quantum Chem.* **101**, 506 (2005).
- [115] D. Lee, F. Furche, and K. Burke, *J. Phys. Chem. Lett.* **1**, 2124 (2010).
- [116] A. Ruzsinszky, J. P. Perdew, G. I. Csonka, O. A. Vydrov, and G. E. Scuseria, *J. Chem. Phys.* **125**, 194112 (2006).
- [117] A. Ruzsinszky, J. P. Perdew, G. I. Csonka, O. A. Vydrov, and G. E. Scuseria, *J. Chem. Phys.* **126**, 104102 (2007).

- [118] G. I. Csonka, J. P. Perdew, and A. Ruzsinszky, J. Chem. Theory Comput. **6**, 3688 (2010).
- [119] A. Ruzsinszky, J. Perdew, and G. Csonka, J. Phys. Chem. A **109**, 11015 (2005).
- [120] J. Tao, J. P. Perdew, and A. Ruzsinszky, Proc. Natl. Acad. Sci. U. S. A. **109**, 18 (2012).
- [121] S. Grimme, J. Antony, S. Ehrlich, and H. Krieg, J. Chem. Phys. **132**, 154104 (2010).
- [122] A. Bondi, J. Phys. Chem. **68**, 441 (1964).
- [123] E. R. Johnson, P. Mori-Sanchez, A. J. Cohen, and W. Yang, J. Chem. Phys. **129**, 204112 (2008).
- [124] A. Savin, *talk at Challenges in Density Matrix and Density Functional Theory*, Gent, Belgium, April 2012.
- [125] B. Civalleri, D. Presti, R. Dovesi, and A. Savin, Chem. Modell. **9**, 168 (2012).
- [126] R. Peverati and D. G. Truhlar, J. Chem. Theory Comput. **8**, 2310 (2012).

# Biography

The author received his B.S. in physics at Shanghai Jiaotong University in China in 2007. Then, He was admitted in department of physics to begin his Ph.D study in 2007. He has been studying density functional theory with Professor John Perdew. He has published four papers during his Ph.D study.

**P. Hao**, J. Sun, B. Xiao, A. Ruzsinszky, G. I. Csonka, J. Tao, S. Glindmeyer, and J. P. Perdew, “*Performance of meta-GGA Functionals on General Main Group Thermochemistry, Kinetics, and Noncovalent Interactions*”, J. Chem. Theory Comput. DOI: 10.1021/ct300868x (2012)

**P. Hao**, Y. Fang, J. Sun, G. I. Csonka, P. H. T. Philipsen, and J. P. Perdew, “*Lattice constants from semilocal density functionals with zero-point phonon correction*”, Phys. Rev. B, 85, 014111 (2012)

J. P. Perdew, J. Tao, **P. Hao**, A. Ruzsinszky, G. I. Csonka, and J. M. Pitarke, “*Spherical-shell model for the van der Waals coefficients between fullerenes and/or nearly-spherical nano-clusters*”, J. Phys. Condens. Matter 24, 424207 (2012).

J. Sun, M. Marsman, G. I. Csonka, A. Ruzsinszky, **P. Hao**, Y.-S. Kim, G. Kresse, and J. P. Perdew, “*Self-consistent meta-generalized gradient approximation within the projector-augmented-wave method*”, Phys. Rev. B 84, 035117(2011).